Properties of HF RADAR Compact Antenna Arrays and Their Effect on the MUSIC Algorithm

Tony de Paolo
Scripps Institution of Oceanography, La Jolla, California

Eric Terrill
Scripps Institution of Oceanography, La Jolla, California

November 9, 2007

Abstract *– Detailed analysis of the compact antenna array patterns and the internal signal processing within the MUSIC algorithm leads to a goodness-of-fit quality metric for the output radial current velocities and bearings produced by the HF RADAR system. To achieve this, some theory behind the MUSIC direction finding algorithm, describing its Direction of Arrival (DOA) metric, is first presented. MATLAB simulations are conducted and statistics are collected on the DOA metrics. The magnitudes of these metrics are directly related to the quality of the bearings produced by the MUSIC algorithm. This research provides HF RADAR users with a practical quality metric for the radial current velocities and their associated bearings produced by the HF RADAR system. Eliminating data with low DOA metrics can decrease the RMS error (by an average of 2.33 cm/s) in up to 70% of the spatial RADAR grid, however comes at a cost of an increase the RMS error(by an average 1.08 cm/s) in 20% of the same grid.*

Quality of measured antenna patterns is paramount to the accuracy of the MUSIC algorithm bearing output. Ambiguities, as well as other aspects of the measured antenna patterns that are detrimental to quality, are discussed. MUSIC results over land bearings are explained, as well as the clustering of radials along the edges of the antenna patterns near land. Best practices are presented to eliminate all of these effects.

Criteria ("MUSIC parameters") for deciding whether a given MUSIC radial velocity originates from one or two bearings are defined and discussed. Varying the MUSIC parameters can decrease error depending on the expected current being measured. A current that generates a majority of radial velocities from only one bearing should have the MUSIC parameters set to favor single bearing solutions, and vice-versa. Simulation results are provided in the Appendices.

1. Introduction

Perhaps the single most important aspect of determining ocean currents using a compact array HF RADAR is the definition of the three antenna patterns as a function of azimuth (bearing) angle. Theoretically, these antenna patterns define an antenna manifold in M-space (in most cases M=3). It is the job of the MUSIC algorithm to: 1) determine a signal space by diagonalization of a covariance matrix formed from the measured signals on each antenna, and 2) determine the most likely signal bearing by projecting all the

points (bearings) of the antenna manifold onto that signal space. The signal space that the MUSIC algorithm determines is a K-dimensional ($K \leq M-1$) subspace of the M-space. The points of the antenna manifold are taken bearing by bearing (usually in 5 degree increments) and projected onto the signal space, and the point in the manifold that has the largest projection onto the signal space determines the bearing(s) from which the signal(s) came. The projection, or how "close" the antenna manifold is to the signal space, can be analyzed to determine a goodness-of-fit metric. This provides quality metrics for MUSIC algorithm solutions that can lead to better definition of overall data accuracy.

2. Ideal Antenna Patterns

The MUSIC algorithm depends greatly on the sensors, or antenna gain and phase patterns. The compact array consists of two dipoles (Antenna 1 and Antenna 2), and one monopole (Antenna 3). The ideal Antenna 3 pattern has unity gain and zero phase in all directions, so the received signal is passed directly through to the receiver with no amplitude or phase distortion. The ideal antenna patterns of the compact array dipoles are generated by (1) picking a pointing angle for maximum gain, and (2) using the cosine of bearing relative to that angle to generate the full antenna pattern. For example, if we assume we are operating on the Pacific coast of the U.S., the coastline runs north-south, and the Pacific Ocean lies between the bearings of 180 and 360. For Antenna 1, we pick a pointing angle of 225 degrees. For Antenna 2, we pick a pointing angle of 315 degrees. The three ideal antenna patterns are shown in Figure 1.

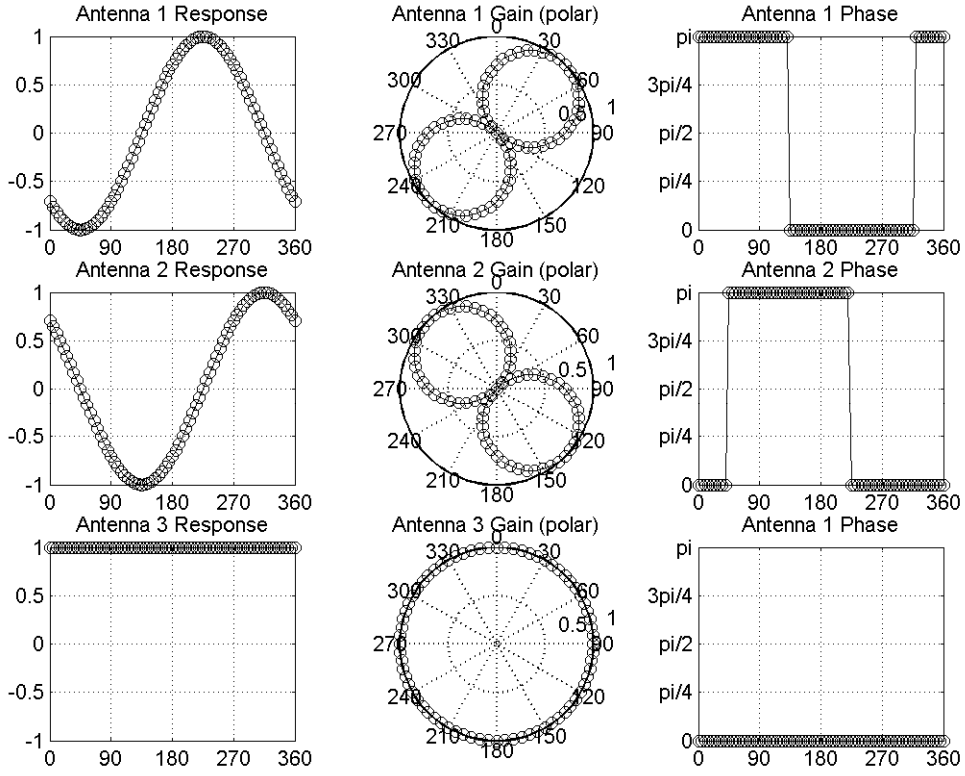

Figure 1 – Ideal Compact Array Antenna Patterns

One can see by the patterns, which are defined in 5 degree bearing increments, that at a given bearing (θ) each antenna has a given magnitude (gain) and phase response. In order to develop the mathematical theory, each antenna response is represented as a complex number

$$A_i(\theta) = |A_i| e^{j\phi_i} \quad i = 1,2,3$$

And the three responses are grouped together to form a point on the antenna manifold

$$A(\theta) = (A_1, A_2, A_3).$$

In the case of the ideal patterns, the complex numbers can be represented by purely real numbers (as in the "Response" plots in Figure 1) since the phase of all the antennas only take on values of 0 or π. For the bearing angles with antenna phases of 0 or π, the exponentials are evaluated as a positive or negative one, and multiply the gain patterns to give real valued antenna responses. In general, with actual measured antenna patterns, this is not the case, which will be discussed in the next section.

2.1 The Antenna Manifold Using Ideal Antenna Patterns

In the idealized antenna pattern case used herein, each antenna pattern gives rise to an orthogonal axis in and M dimensional vector space. In our case, M=3. The antenna patterns are indeed orthogonal to each other with respect to bearing angle. This can be shown by pair wise correlation of the patterns over bearing

$$\int_0^{2\pi} \cos(\varphi + \frac{\pi}{4}) \cdot \cos(\varphi + \frac{3\pi}{4}) d\varphi = 0$$

$$\int_0^{2\pi} 1 \cdot \cos(\varphi + \frac{\pi}{4}) d\varphi = 0$$

$$\int_0^{2\pi} 1 \cdot \cos(\varphi + \frac{3\pi}{4}) d\varphi = 0$$

These antenna patterns form an orthogonal basis for a 3 dimensional vector space, with each axis representing the response of each antenna. Furthermore, if we parameterize the three individual antenna responses as a function of bearing angle, 3 dimensional vectors are formed using each bearing, and an antenna manifold is created over all bearings, shown in Figure 2.

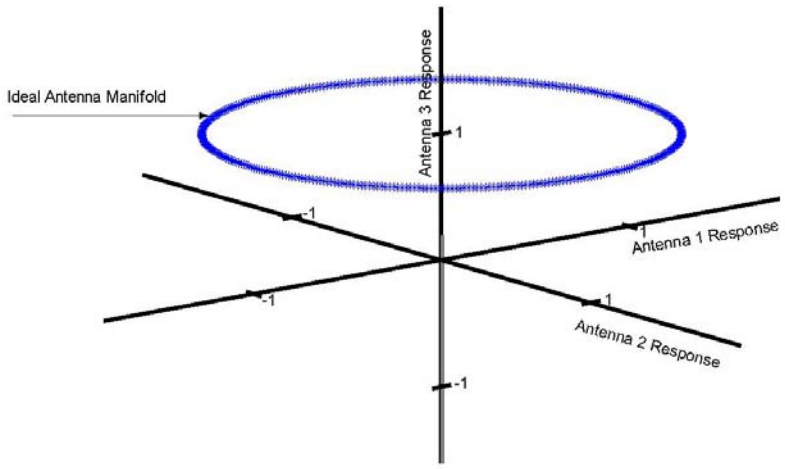

Figure 2 – Ideal Antenna Manifold in a 3-Dimensional Vector Space

This antenna manifold produced from ideal antenna patterns can be displayed in 3 dimensions since all of the antenna responses are real numbers. In practice, the response of each antenna at each bearing is a complex number, with magnitude and phase; hence the antenna manifold is comprised of 3-dimensional vectors with each component being complex, which cannot be plotted so easily.

3. The Covariance Matrix, and its M-dimensional Basis

Given M sensors (antennas) an MxM covariance matrix of the received antenna voltages is generated. 512 point complex sample vectors are taken from each antenna, and complex FFTs are performed on each (generating 512 frequency bins). The resulting complex spectra are auto and cross multiplied bin by bin and averaged (for full details see Appendix). Each resulting frequency bin gives rise to a 3x3 covariance matrix of the measured signals at that frequency

$$C = \begin{vmatrix} C_{11} & C_{12} & C_{13} \\ C_{21} & C_{22} & C_{23} \\ C_{31} & C_{32} & C_{33} \end{vmatrix} = \begin{vmatrix} \langle S_{11}(n) \rangle & \langle S_{12}(n) \rangle & \langle S_{13}(n) \rangle \\ \langle S_{12}(n) \rangle^* & \langle S_{22}(n) \rangle & \langle S_{23}(n) \rangle \\ \langle S_{13}(n) \rangle^* & \langle S_{23}(n) \rangle^* & \langle S_{33}(n) \rangle \end{vmatrix}$$

The covariance matrix represents one Doppler cell of the averaged cross spectra of the three received signals. The inherent problem is that the signals in each Doppler cell (the frequency of which is a combination of Bragg scatter plus Doppler due radial current velocity) are really summations of signals from all bearings (plus noise), hitting each antenna. The bearing angle from which the received signal comes is still unknown. To figure out the bearing angle, first the covariance matrix must go though eigenvalue decomposition (diagonalization) to estimate a signal subspace and the noise subspace. But first, let's try and visualize what dimension and shape the subspaces have.

3.1 Signal Subspace

As a graphical example of the signal subspace with ideal antenna patterns, Figure 3 analyzes a signal emanating from a point source at a bearing of 225 degrees. This signal will give rise to 3-tuple of voltages on the three antennas, **S1 =** α**A(**225**)**, a linear multiple of the antenna responses at that bearing (note that α can be a complex constant). Given antenna 3 has unity gain, the actual magnitude and phase of the signal will be received there. While on antennas 1 and 2, the magnitude and phase of the signal will be modified depending on the bearing and the antenna patterns at that bearing. This is represented in M-space as vector **S1**, from the origin, going through the antenna manifold at the bearing from where it came. The magnitude and phase of this signal can change with time, but (given that the source of the signal is stationary) the bearing cannot. This signal vector lies in a one dimensional signal subspace. Any signal from that one bearing lies in that 1-dimensional subspace, a line. Figure 3 shows the **S1** signal vector sticking out of the page along the positive A1 axis, also shown is the location on the manifold from a zero degree bearing input.

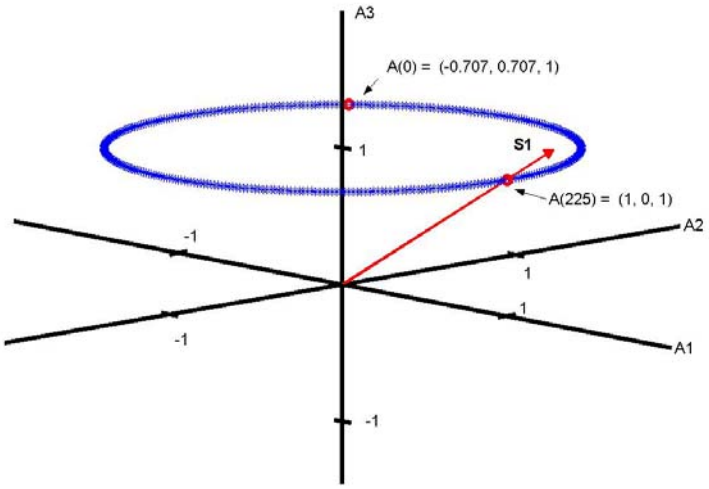

Figure 3 - Signal S1 from Bearing 225 along a 1-Dimensional Signal Subspace

Now consider a signal **S2 =** β**A(**270**)** with the same characteristics (in our case, the same Doppler shift, from the same radial current velocity) emanating from a second bearing 270. This signal can likewise be represented by a vector from the origin through the antenna manifold at a bearing of 270. These two vectors, **S1** and **S2**, lie in a 2-dimensional signal subspace, or plane. Figure 4 shows the **S1** and **S2** signal vectors in the signal subspace plane (a higher elevation viewpoint of the manifold helps with the visualization).

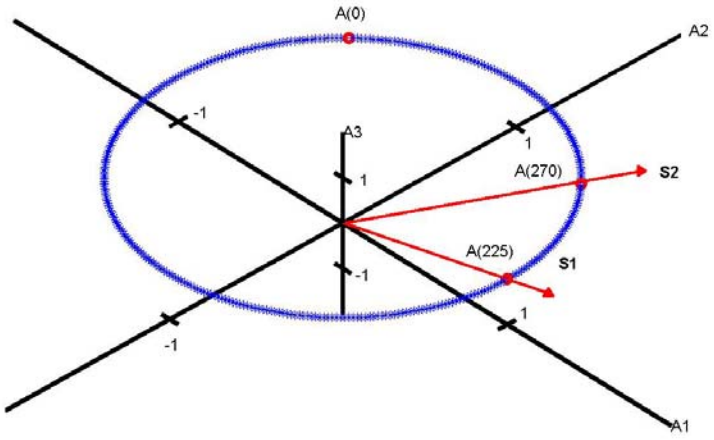

Figure 4 - Signal S1 from Bearing 225 and S2 from Bearing 270 in a 2-Dimensional Signal Subspace

Thus with ideal antenna patterns and no noise, the signal space picture is easy to define and visualize. Under more realistic conditions, the antenna manifold has complex vector components, the signals are complex, and contain additive Gaussian noise. Covariance matrix decomposition will determine the dimensionality and direction of the signal subspace, but first we define the noise subspace.

3.2 Noise Subspace

There are two sources of noise in a practical HF radar system:

1. system (thermal) noise generated by the receiving equipment, and
2. the spatial noise field (in our case, the combination of the wind wave noise and the current noise, both modeled as Gaussian).

The system noise should be independent from antenna to antenna, so that if no signals were present, there would be no correlation between the samples taken from the three antennas. Considering our vector of 512 samples at approximately 2 Hz, the system generates a 3-tuples of noise every sample $w_n, n = 1,2,...512$. If we cross-correlate the noise samples from the individual sensors to form a covariance matrix Σ_0, this matrix would be diagonal, and would be given by $\Sigma_0 = \sigma^2 I$, where σ^2 is the (zero mean) noise variance. The received noise vectors w_n are of equal strength and random with respect to bearing, they have no direction with respect to the array manifold. They can be visualized in the 3-dimensional vector space as occupying a sphere about the origin as shown in Figure 5.

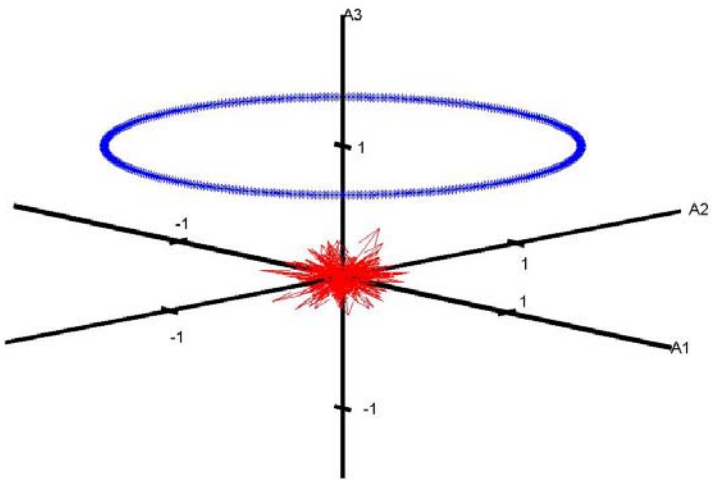

Figure 5 - Uncorrelated Noise Vectors are Non-directional with Respect to Bearing

The assumption in the SeaSonde simulation is that the noise is uncorrelated with respect to bearing. Again, covariance matrix decomposition will determine the dimensionality and direction of the noise subspace.

3.3 Eigenvalue Decomposition

To determine the signal and noise subspaces, the covariance matrix goes through eigenvalue decomposition. This diagonalization produces 3 eigenvalues, ordered largest to smallest, and three corresponding eigenvectors. The eigenvectors form a 3-dimensional orthonormal basis. An estimate of the signal subspace comes from the eigenvectors corresponding to the largest eigenvalues. First assuming that there is only one signal from one bearing present, the first eigenvector (largest eigenvalue) defines a 1-dimensinonal signal subspace (ala **S1**). The remaining two eigenvectors are then assumed to be associated with noise, and define a 2-dimensional noise subspace. The signal and noise subspaces are orthogonal to each other.

Additionally, if it is assumed that there are two signals from two different bearings, the first two eigenvectors define a 2-dimensional signal subspace (ala **S1** and **S2**), and the remaining eigenvector defines a 1-dimensional noise subspace (again orthogonal).

Now that the signal and noise subspaces have been estimated, the process of determining which part of the antenna manifold is a best fit to the estimated signal subspace is performed. This in turn provides the best estimate of signal bearing, the final result.

4. The Direction of Arrival (DOA) Function

4.1 Antenna Manifold Projections

The crux of the MUSIC algorithm is that not only is the signal subspace eigenvector orthogonal to the noise subspace eigenvectors, but also there is an antenna manifold vector (being a linear multiple of the signal) that is also orthogonal to the noise subspace eigenvectors. Due to the noise incorporated in the covariance matrix, our estimate of the noise subspace will not be exactly orthogonal to the antenna manifold vector, but perhaps close. Just how close needs to be determined. In fact, the MUSIC algorithm takes each antenna manifold vector (one from each bearing) and projects it onto the estimated noise subspace. If any of the antenna manifold vectors were truly orthogonal to the noise subspace, then the projection would be zero. The bearing that produces the antenna manifold vector with the smallest projection onto the noise subspace is the best estimate of the signal bearing.

Keeping with the previous single signal example S1, Figure 6 shows a small (real) noise vector N1 is added to produce a received signal plus noise vector R1.

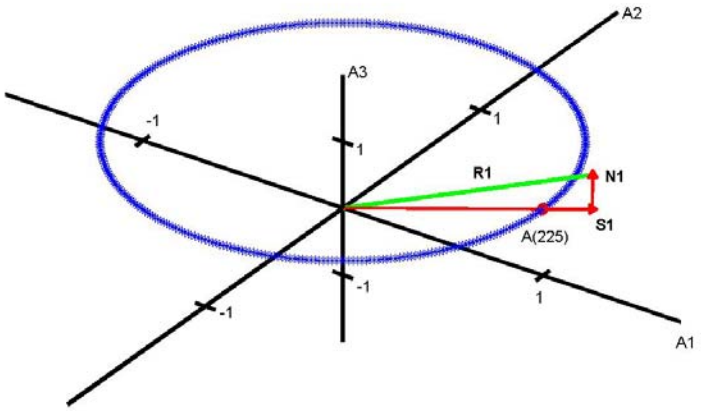

Figure 6 – Received signal plus noise vector R1

This received signal might give rise to a covariance matrix similar to

$$C = \begin{bmatrix} 0.2162 & 0.0303 - 0.0090i & 0.3170 - 0.0063i \\ 0.0303 + 0.0090i & 0.0436 & -0.0091 + 0.0213i \\ 0.3170 + 0.0063i & -0.0091 - 0.0213i & 0.5416 \end{bmatrix}$$

with an eigenvalue decomposition.

$$
\begin{aligned}
C &= E\Lambda E^{-1} \\
&= \left[E_1 E_2 E_3\right]\Lambda E^{-1} \\
&= \begin{bmatrix} 0.6916 - 0.0499i & 0.4957 + 0.0432i & 0.5212 - 0.0087i \\ -0.5785 + 0.0956i & 0.8084 - 0.0392i & 0.0117 + 0.0326i \\ -0.4189 & -0.3121 & 0.8527 \end{bmatrix} \begin{bmatrix} 0.0001 & 0 & 0 \\ 0 & 0.0653 & 0 \\ 0 & 0 & 0.7362 \end{bmatrix} \begin{bmatrix} 0.6916 + 0.0499 & -0.5785 - 0.0956 & -0.4189 \\ 0.4957 - 0.0432 & 0.8084 + 0.0392 & -0.3121 \\ 0.5212 + 0.0087i & 0.0117 - 0.0326i & 0.8527 \end{bmatrix}
\end{aligned}
$$

The columns of E = [E_1 E_2 E_3] are the eigenvectors of C, the diagonal elements of Λ are the eigenvalues. The largest eigenvector from the largest eigenvalue (λ_3) provides the estimate of the 1-dimensional signal subspace (E_3) (dashed line). The other two eigenvectors E_1 and E_2 form the 2-dimenesional noise subspace (yellow plane). For illustration purposes the normalized real parts of the eigenvectors (unit length) are used in Figure 7 to plot out these subspaces.

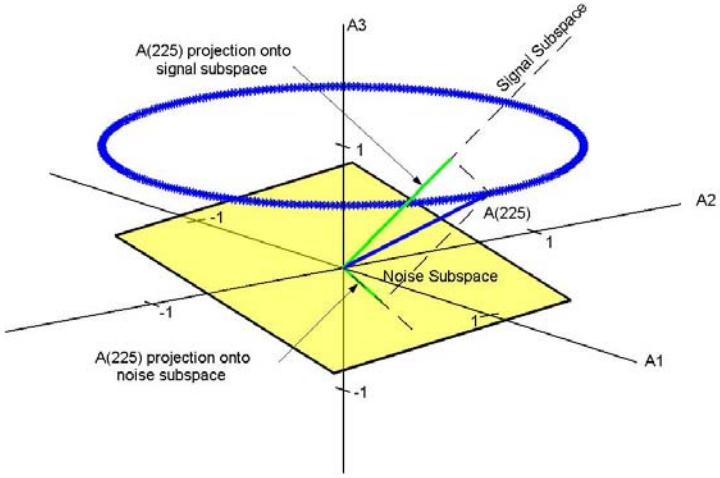

Figure 7 – Projections of antenna manifold point A(225) onto the estimated signal/noise subspaces

Given that the eigenvectors above, and A(225) = (1, 0, 1), the magnitude of the projections (solid green lines) onto the signal and noise subspaces are 1.88 and 0.11 respectively. These are the maximum and minimum projections for the covariance matrix in this example; therefore it is assumed that the bearing angle associated with this signal is 225 degrees.

One more hypothesis to consider is that the signal subspace is 2-dimensional and the noise subspace 1-dimensional. In this case the shapes of the two subspaces are interchanged in Figure 7 and a different picture is produced. Since it is now assumed that the signal subspace is 2-dimensional, the two smallest projections of the antenna manifold onto the 1-dimensional noise subspace are found, and the two bearings corresponding to those two minima are assumed to be the signal bearings. These bearings are 205 and 330, which give A(205) = (0.9397, 0.3420, 1) and A(330) = (-0.2588, -0.9659, 1).

Looking first at bearing 205, Figure 8(a) shows A(205) in blue, the signal subspace as a white plane (black outline), the perpendicular noise subspace as a dashed yellow line, and the projection of A(205) onto the noise subspace. Figure 8(b) shows A(330) and it's projection onto the noise subspace. Both A(205) and A(330) nearly lie in the signal subspace plane, and their projections onto the perpendicular noise subspace are small values of 0.0011 and 0.0015 respectively. They are difficult to see in Figure 8 and the axes in both plots have been rotated to give the best possible view.

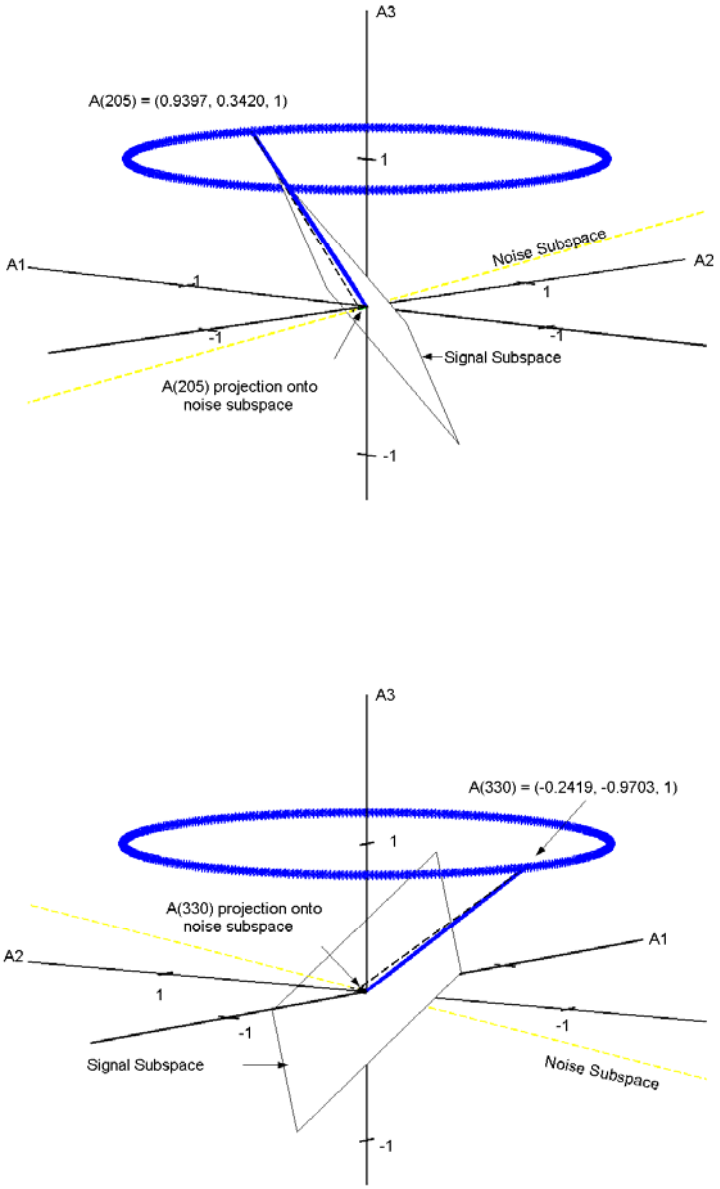

Figure 8 - (a) Projection of antenna manifold point A(205) onto the estimated noise subspace, and (b) projection of antenna manifold point A(330) onto the estimated noise subspace

4.2 DOA functions for 1- and 2-Dimensional Signal Subspaces

Since the eigenvectors that define the signal and noise subspaces have unit length, and as defined, the antenna manifold vectors are of length sqrt(2), then the squared magnitude of the projection of any antenna manifold vector onto the estimate of either subspace is within the interval [0, 2]. Rather than consider the signal space projections over all bearings and look for a maximum, the MUSIC algorithm considers all the noise subspace projections and looks for a minimum. The direction of arrival (DOA) function is generated which provides the reciprocal of the squared magnitude of the projection onto the noise subspace

$$DOA(\theta) = \frac{1}{A^*(\theta)E_n E_n^* A(\theta)}$$

(1x3) (3xm) (mx3) (3x1)

where E_n are the eigenvector(s) defining with the noise subspace
$A(\theta)$ and $A(\theta)^*$ are the antenna vectors and conjugate transposes
m = 1, 2 is the assumed dimension of the noise subspace

The noise subspace projection is in the denominator, therefore the DOA function goes to infinity when the projection is zero, or when the antenna manifold vector is exactly orthogonal to the noise subspace. For the example, 10*log(DOA(θ)) under the 1-and 2-dimensional signal space hypotheses are plotted in Figure 9.

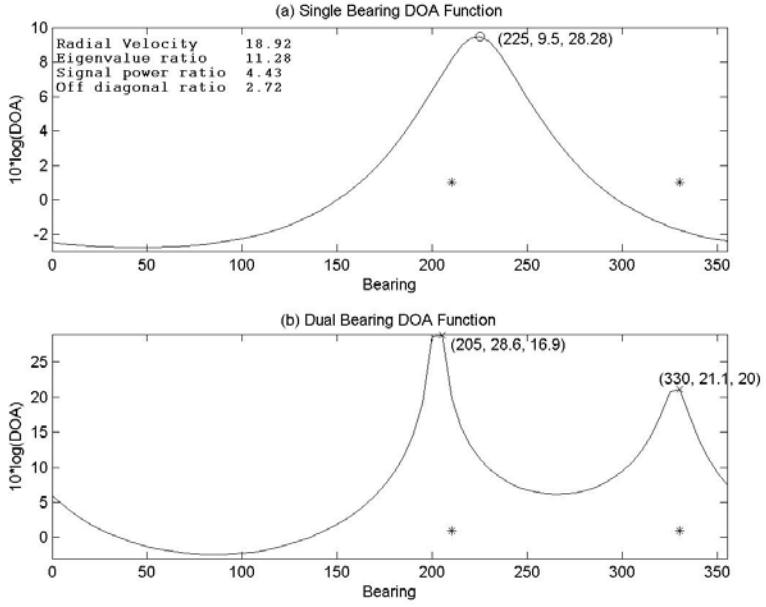

Figure 9 – DOA functions assuming (a) 1-dimensional signal space and (b) 2-dimensional signal space

In Figure 9(a), the maximum of the DOA function is at bearing 225 and has a value of 10*log(1/0.11) = 9.5 dB. Other information on the plot includes the deterministic radial velocity associated with the Doppler cell (and this covariance matrix) of 18.92 cm s^{-1} and other signal metrics that will be examined later. The label at the peak shows the bearing of 225 degrees, the maximum DOA metric of 9.5 dB, and the radial velocity of the input at that bearing of 28.28 cm s^{-1}, which is roughly a 10 cm s^{-1} error for this output at 225 degrees. The asterisks show where there were input radial velocities near the Doppler cell radial velocity, closer to 210 degrees bearing. So one can look at this error in two ways, either assume the bearing is correct and call it a 10 cm s^{-1} radial velocity error, or assume that the radial velocity is correct and call it a 15 degree bearing error. Notice that there is another asterisk at 330 degrees, indicating another bearing where the radial current velocity input comes from in this Doppler cell.

Looking at Figure 9(b), the dual bearing DOA function shows maxima at 205 and 330 degrees. These MUSIC outputs are within 2 cm s^{-1} of the radial current velocity for this Doppler cell, and are a better result. The two peaks have DOA metrics of 28.6 and 21.1 dB respectively, which are much greater than the DOA metric for the single bearing solution (9.5 dB). However, the dual bearing solution was not chosen in this case due to the other signal metrics previously mentioned. These other metrics and their implications are discussed later.

4.3 Statistics of the DOA function

Given the magnitude of the error in the single bearing solution above, one would hope to modify the MUSIC algorithm parameters to choose the better dual bearing solution. Assuming for now that we're stuck with the solution as it stands, what information can we glean from the DOA function that might provide a quality assessment of the result? Using the MATLAB simulation developed in (de Paolo and Terrill, 2007), with simulated eddy current shown in Figure 10(a), the radial projections shown in Figure 10(b), the MUSIC algorithm produces the radial results show in Figure 10(c). These results are from 1 hour of simulated input data, or 6 "10-minute" cross-spectra.

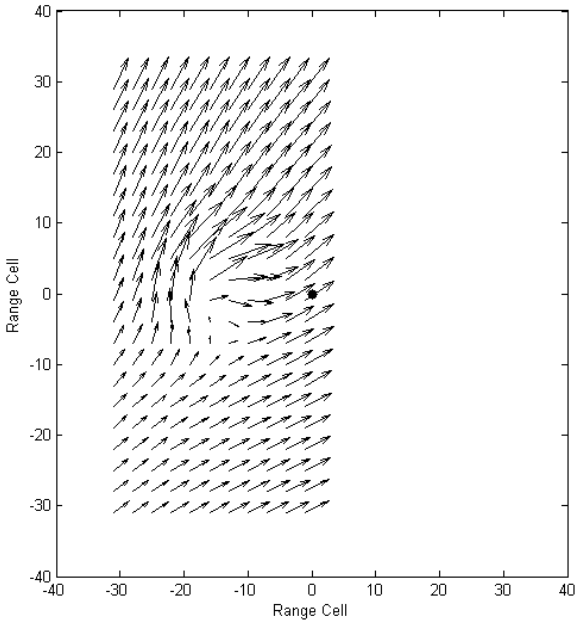
Range Cell
Range Cell
40
30
20
10
0
-10
-20
-30
-40
-40
-30
-20
-10
0
10
20
30
40

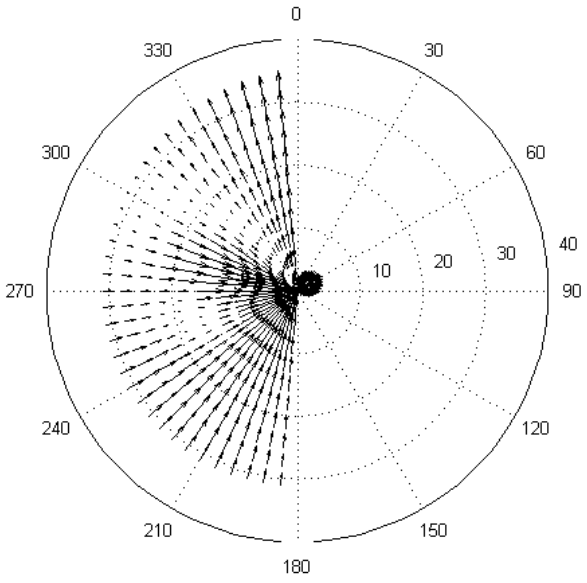
0
30
60
90
120
150
180
210
240
270
300
330
10
20
30
40

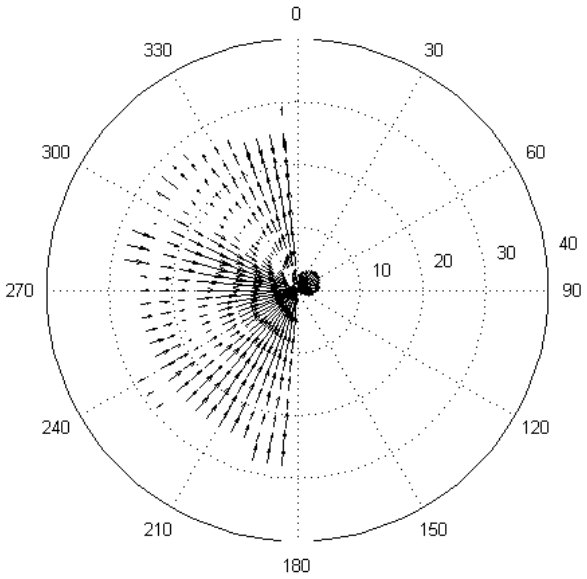

Figure 10 – (a) input eddy current, (b) input radial projection, and (c) MUSIC radial current velocity output

Collecting DOA metrics for these MUSIC solutions (both single and dual bearing), statistics are gathered and shown in Figure 11. A full set of statistics for many different input currents, input current noise levels, and wind directions is given in Appendix A.

The second plot 11(a) show the distribution of the DOA metric values collected over the hour. These values are the maxima of the DOA functions as shown in Figure 9. Both the single and double bearing solution metrics are grouped together for this plot. The mean of the distribution is 23.77 dB, with a standard deviation of 10.96 dB. A higher metric indicates a "better fit", the projection of the received signal on to the estimated signal space is larger, "fitting" the antenna manifold well at the resultant bearing angle. Conversely, a lower metric indicates a "poor fit" of the received data to the antenna manifold. Much higher DOA metrics are certainly better, however the DOA metrics around zero are certainly worse. We will use the magnitude of the DOA metric for each result as a "goodness-of-fit" quality metric, and provide it with the radial data.

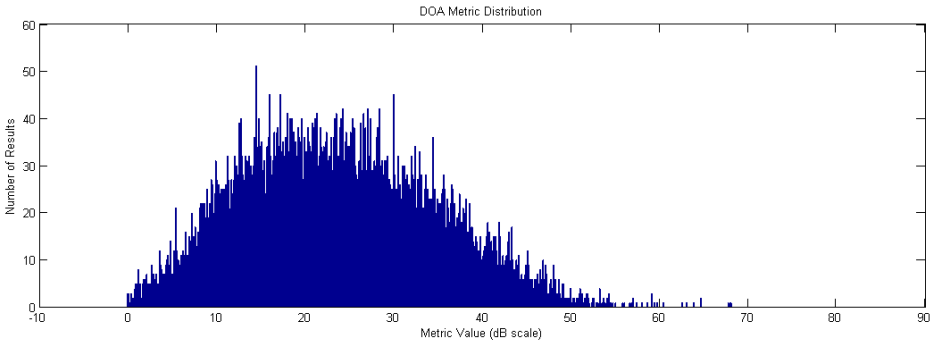

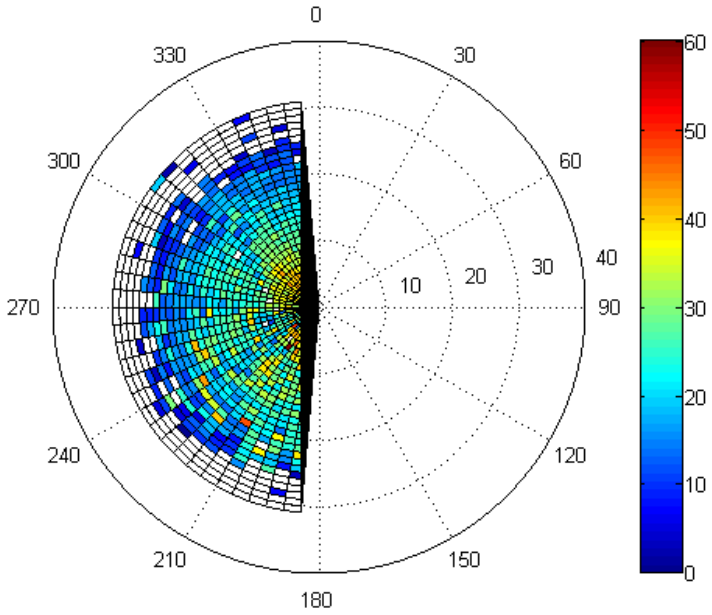

Figure 11 – (a) statistical distribution of the DOA metric values, (b) spatial distribution of DOA metric values

The second plot 11(b) shows the spatial distribution of the DOA metric. This shows areas of potential poor data quality where the metrics are low (blue). As expected, the DOA metrics get lower as range increases and SNR decreases. There are isolated pockets at close range that also show a low DOA metric value.

4.3.1 Definition of Errors

We want to find if the DOA metric is a quality indicator for either radial velocity error or bearing error in the MUSIC solutions. First we need to define some statistics related to quality:

1. Radial velocity error is the RMS difference between the MUSIC radial velocity output and the simulated input for that (R, θ) cell

2. Bearing error is computed as the difference in bearing (in 5 degree increments) to the nearest radial velocity input that is within +/-5 cm/s of the input radial velocity

The tolerances for radial velocity and bearing errors were chosen to coincide with expectations of the HF RADAR community, they are up for debate. For now, using these definitions of error, we can plot them vs. DOA metric value, shown in Figure 12. Using an hours' worth of data, one can see that the average radial velocity error and average bearing error both go down as DOA metric increases, validating the DOA metric's usefulness as a measure of data quality.

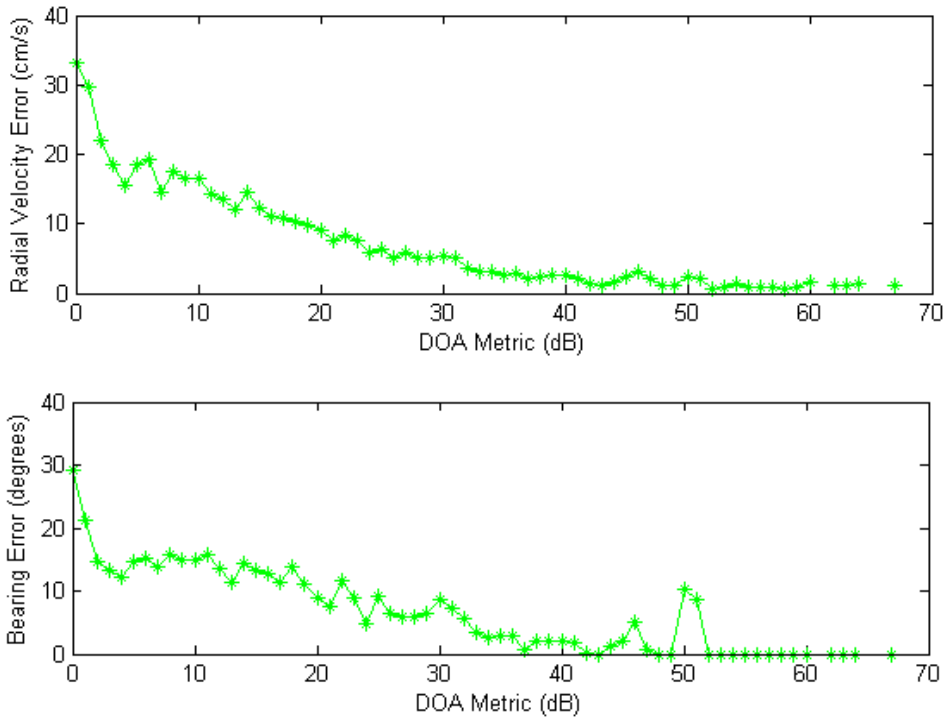

Figure 12 – (a) Radial velocity error vs. DOA metric, (b) bearing error vs. DOA metric, showing average decrease in both errors as DOA metric increases

4.3.2 Definition of True/False Positive Results

As additional statistics for use in determining the quality of MUSIC output, we define:

1. A True Positive result is a radial velocity output within +/-5 cm/s of the simulated radial velocity input, for that (R, θ) cell OR its bearing neighbors (within +/-10 degrees)

2. A False Positive result is the set of results in the complement of the set of True Positive results, including all results over land

The idea being that MUSIC output that is "close enough" to the radial current velocity input will be regarded as a "true positive" result.

4.4 Effects of Eliminating Results with Low DOA Metrics

4.4.1 Skill

We can now start throwing away results with low DOA metrics and see how it affects various error statistics. Eliminating any MUSIC result that has a DOA metric of less than 10 dB and then comparing skill metrics for the results, we get Figure13.

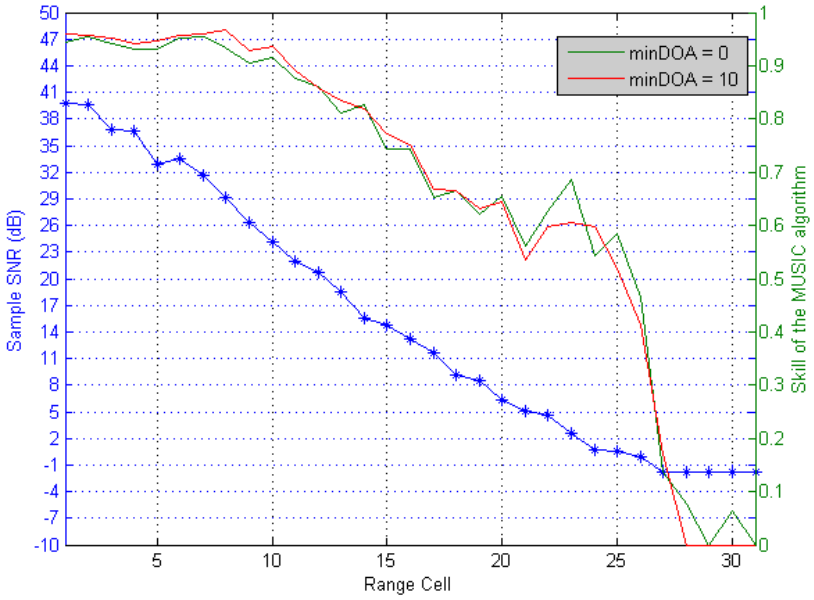

Figure 13 – Skill comparison using all MUSIC results (green) vs. only MUSIC results with DOA metrics of 10 dB or greater (red)

One can see three effects in Figure 13:

1. In general, slightly higher skill when low DOA metric results are eliminated
2. Lower skill in some range cells (20-23 for example), even when eliminate low DOA metric results. This shows that it is not always a good idea, however this is seen when the SNR is low, and results are more random in general.
3. A reduction in range, since low DOA metrics tend to accompany low SNR, and are eliminated.

4.4.2 True/False Positive Ratio (TP/FP)

Perhaps a better effect of eliminating low DOA metric results is seen in the change in the number of False Positive and True Positive results in Table 1.

DOA Minimum	FP	TP	TP/FP
0	1452	8795	6.06
10	1102	8062	7.32

Table 1 – Comparison of the number of False Positive Results vs. True Positive results when eliminating results with DOA metrics of 10 dB or less

One can see a general reduction in the total number of results, as expected, however the ratio of True Positive to False Positive results go up. This occurs in all tested current cases, which are summarized in Appendices A.1 and A.2.

4.4.3 RMS Error and Coverage

The best visualization of the effects of eliminating low DOA metric results is seen in the decrease of RMS error over the spatial field (which unfortunately is accompanied by a decrease in coverage) as seen in Figure 14. Using a simulated uniform onshore current as input, radial velocity MUSIC results were eliminated under a range of DOA metric cutoffs, varying from 1 to 20, over 20 different runs. That is, the first simulation run eliminated all results with DOA metrics of 1 dB and below, the second run eliminated all results with DOA metrics of 2 dB and below, etc. Results were then tabulated for each (R, θ) cell in the spatial field. When all DOA metrics are accepted, that represents "100%" coverage. The x-axis is the DOA metric cutoff, and the y-axis is the percentage of (R, θ) cells that showed:

1. a decrease in RMS error
2. a increase in RMS error
3. a decrease in coverage

when compared to the "100%" coverage data (DOA cutoff of zero).

One can see a steep rise (blue curve) in the percentage of (R, θ) cells that exhibit a decrease in RMS error. This seems to peak around a DOA metric cutoff of 10 dB. There is also a less steep rise (green curve) in the percentage of (R, θ) cells that exhibit an *increase* in RMS error after elimination of some results. This shows that some MUSIC results with low DOA metrics are actually good results (true positives), but certainly a smaller percentage than those that are bad results (false positives). Considering the elimination of all radial velocity results with DOA metrics of 10 dB and below, there is a 70% increase of (R, θ) cells that have a lower RMS error (2.33 cm/s lower on average). This comes at a cost of a 19% increase in (R, θ) cells that have a higher RMS error (1.08 cm/s on average), and a 2% reduction in coverage.

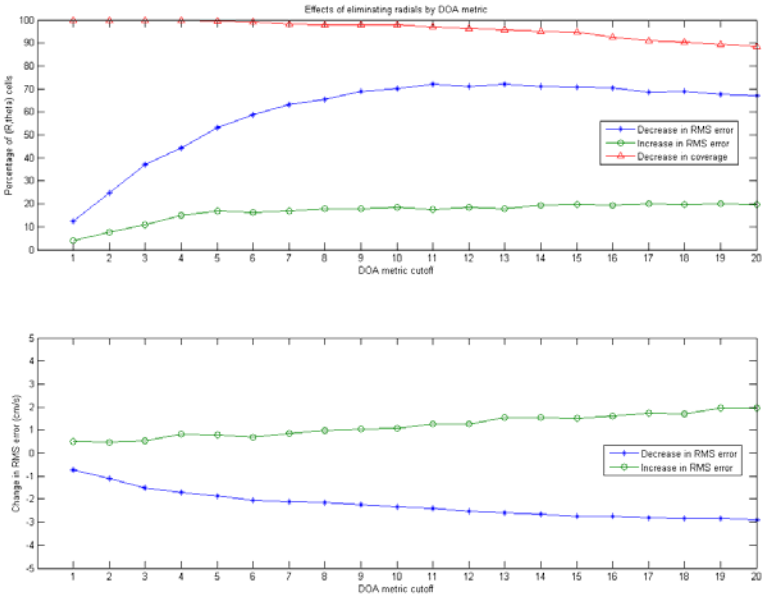

Figure 14 – The effects of eliminating radial velocity results for a uniform onshore current over a range of DOA metric cut off values

As a second example, the eddy current used previously (Figure 10) is used to generate Figure 15. Results for a more complex current are less favorable that those for the uniform current above. Once again examining at 10 dB DOA cutoff value, approximately 48% of (R, θ) cells experience a decrease of RMS error (1.87 cm/s lower on average), 32% have an increase in RMS error (1.8 cm/s higher on average), and the coverage is reduced to 95%.

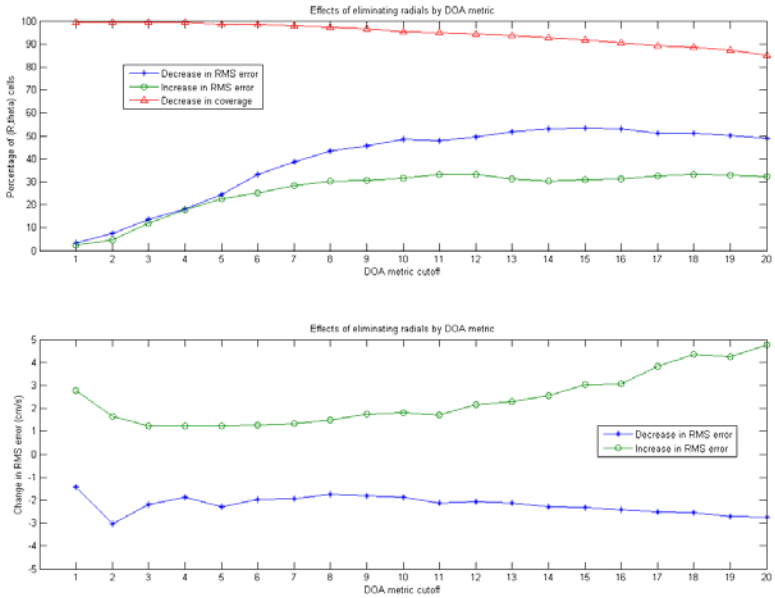

Figure 15 – The effects of eliminating radial velocity results for an eddy over a range of DOA metric cut off values

5. Measured Antenna Patterns

This section develops the effect of measured patterns on the DOA metric and the goodness-of-fit quality metric. Inaccuracies in the measured pattern play a direct role in reducing the quality of the radial results. Measured patterns are examined for ambiguities (a lack of diversity) at certain bearings and how they affect the quality metric.

5.1 Analysis of San Diego Border Park (SDBP) HF RADAR

As a case study, measured antenna patterns from the SDCOOS San Diego Border Park (SDBP) SeaSonde system are analyzed. A problem with the SDBP system was first noticed by Sung Yong Kim while re-processing the cross spectra with both the measured antenna pattern and then again with ideal antenna patterns over many months. Using different antenna manifolds will certainly produce different radial data output, however the general current flow should follow similar directions with similar velocities. He noticed a large discrepancy in the radial velocity output for the bearing sector at 287 degrees. The sector in question can be plainly seen in red in Figure 16. (There are also other areas around Point Loma that have large RMS differences which are under investigation.)

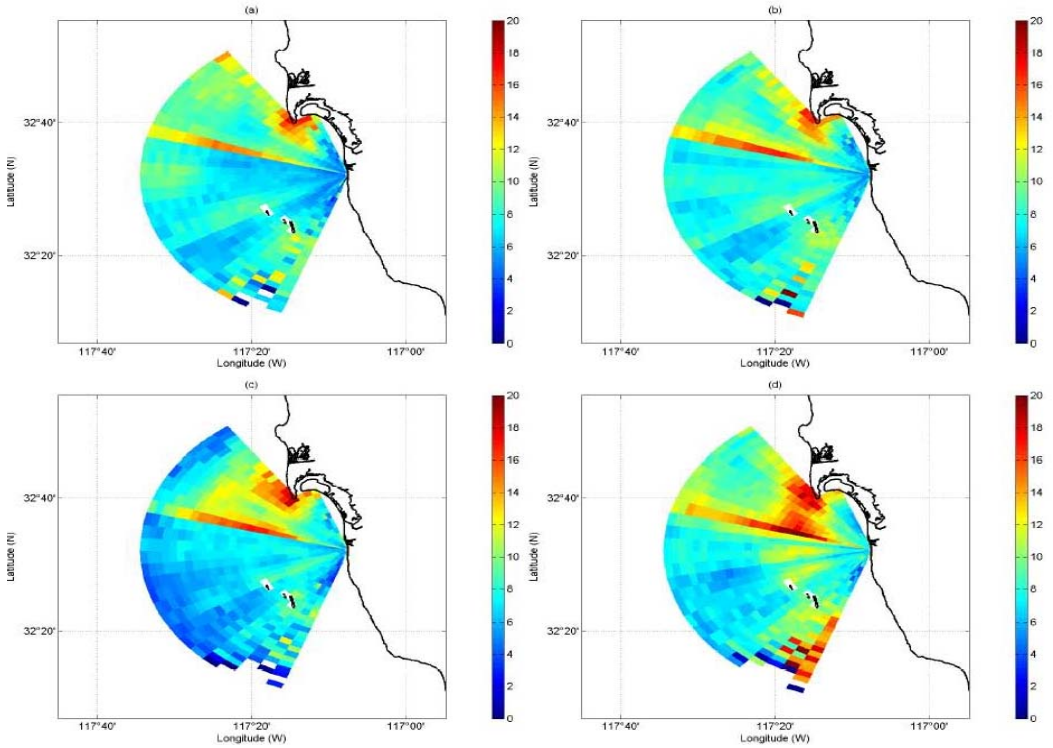

Figure 16 - The root-mean-square difference of radial velocity vectors at SDBP, using measured beam patterns and ideal beam patterns during the month (a) Sep. 2003 (b) Oct. 2003 (c) Feb. 2005 (d) Mar. 2005

To determine the cause of this difference, we first look at the radial velocity output the MUSIC algorithm for both measured and ideal patterns in Figure 17. In general, one can see a positive radial current (toward the RADAR) from the northwest, and a negative radial current (away from the RADAR) toward the southwest. The upper Figure 15(a) shows radial velocity vectors using the measured beam patterns. In the zoomed in breakout on the left, the radials along bearing 287 are going contrary to the general flow around them at other bearings. The lower Figure 15(b) shows radial velocity vectors using ideal beam patterns. The zoomed in area now shows consistent flow with the neighboring bearing sectors. Since the flow is more consistent with the ideal patterns, further investigation into the measure patterns is warranted.

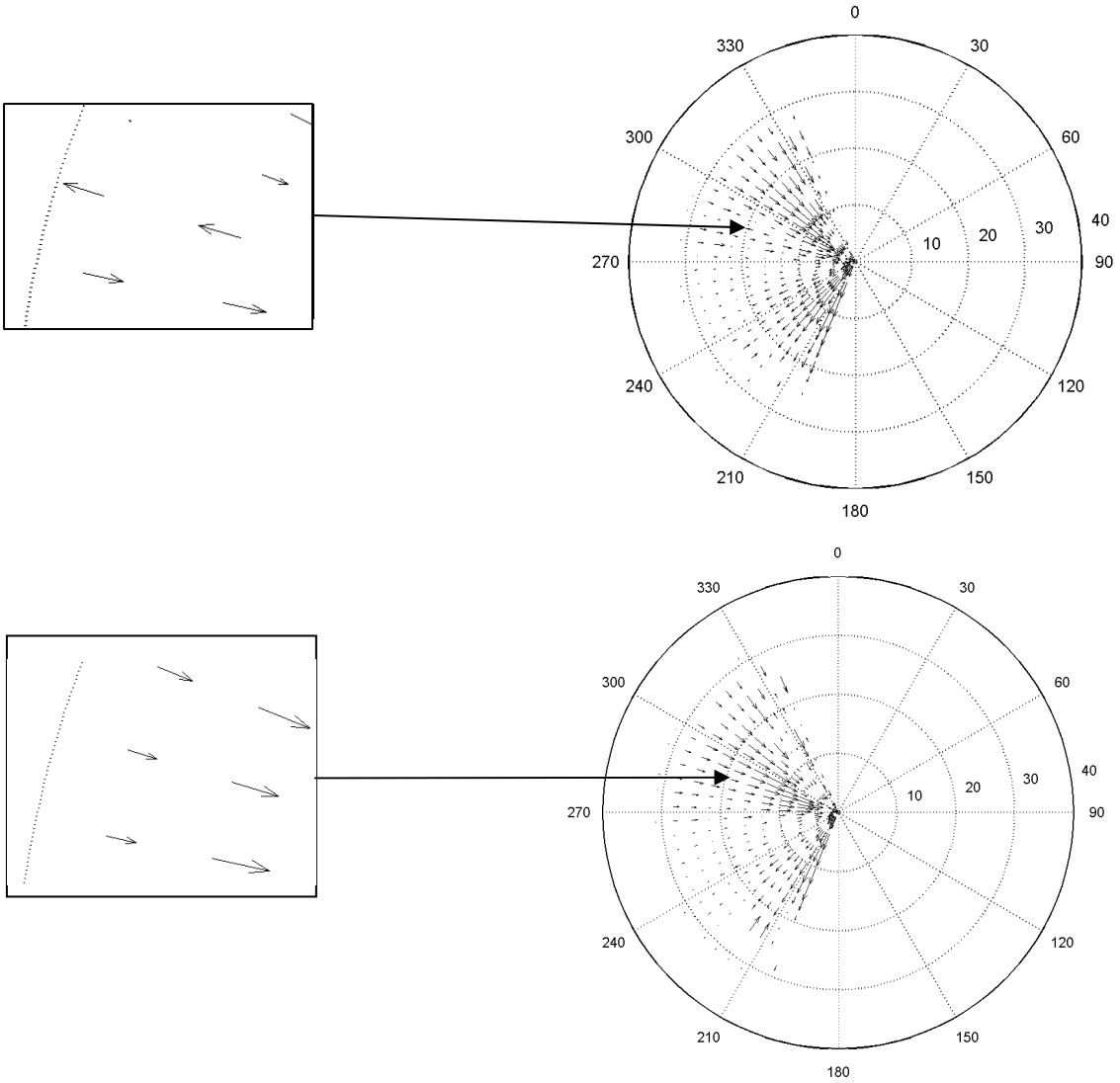

Figure 17 – SDBP radial velocity vector output for (a) measured antenna patterns, and (b) ideal antenna patterns showing opposite flows along bearing 287

5.1.1 SDBP Antenna Patterns

In order to dig deeper into the discrepancy, the SDBP measured antenna patterns are shown in Figure 18.

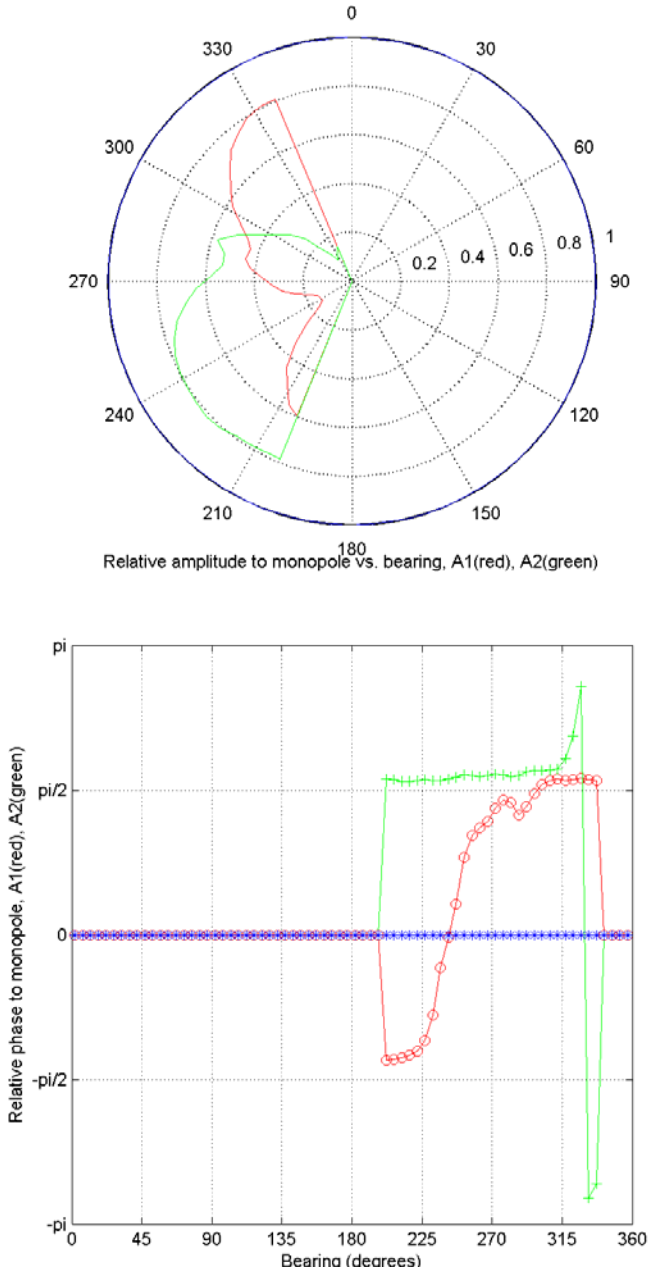

Figure 18 – Relative (a) amplitudes and (b) phases (to the monopole) for the crossed loop antennas (A1, A2) at SDBP

There are irregularities in both the dipole antenna patterns at 287 degrees, which appear as increases in the amplitudes, and there is also a visible phase shift for A1 at that bearing. These irregularities in the measured patterns create a bearing ambiguity for the MUSIC algorithm. That is, the antenna response at one bearing is very close to the antenna response at another. As discussed in previous sections, the projection of the antenna manifold onto the noise subspace will be very similar for two separate bearings, making the DOA metric for both bearings close in value. Subsequently, when searching

for the maxima of the DOA function, either the incorrect single bearing will be chosen, or a dual bearing solution with an incorrect bearing will be produced.

5.1.1.1 SDBP Antenna Pattern Ambiguity Plot

As an indicator of potential antenna pattern ambiguity, we compute the inverse of the squared distance between all the antenna manifold points in signal space. For each bearing in the manifold θ_i and each manifold point $a(\theta_i)$, the inverse of the distance to every other point in the manifold $A(\theta)$, is computed (in dB) using the vector equation

$$D^2 = 10\log_{10}\left(\frac{1}{\sqrt{(a(\theta_i) - A(\theta))^T (a(\theta_i) - A(\theta))}}\right)$$

where ^{T} indicates conjugate transpose.

Every bearing θ_i generates one row of the ambiguity plot, and the plots are symmetric across the diagonal. When this equation computes the inverse of the distance between a point and itself, the result is infinity and therefore limited to an arbitrary value of 16 dB. Figure 19 shows a comparison of and ideal antenna pattern ambiguity plot along side the SDBP antenna pattern ambiguity plot.

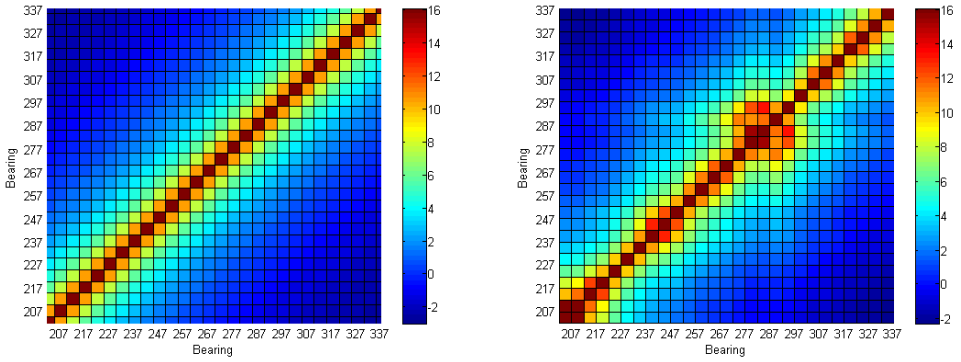

Figure 19 – (a) Ambiguity plot for ideal antenna patterns vs. (b) ambiguity plot for SDBP antenna patterns

With ideal antenna patterns, the ambiguity plot shows a monotonically increasing distance between antenna manifold points as one moves away from the diagonal. With the SDBP antenna patterns, one can see a few areas in the ambiguity plot where the distances between antenna manifold points remain relatively small. This is obvious in our former region of interest around bearing 287 where the reddish region extends beyond the diagonal by roughly 15 degrees of bearing.

These ambiguity plots can be useful in identifying any potential problematic regions in any measured antenna pattern. Once a problematic region is identified, the ambiguities can be mitigated by either artificially smoothing the measured antenna patterns, or by re-measurement. Upon re-measurement of the SDBP antenna patterns, we found that the ambiguous region did not go away, indicating a problem with the antenna installation. As it turned out, metal fencing behind the antenna was to blame, and once removed, rectified the problem.

5.1.2 SDBP DOA Functions

Finally we look at the DOA functions using the SDBP measured antenna patterns in Figure 18. In Figures 20(a,b), the radial velocity output is -16.55 cm s^{-1}, and the single bearing solution is chosen (due to eigenvalue and signal power ratios) giving a bearing of 287. Note the double peak in the single bearing DOA function, this is due to the projection of the antenna manifold onto the noise subspace producing similar results for two different bearings. The irregularity in the measured antenna pattern has made it ambiguous whether to choose bearing 287 or bearing 272 (which we believe to be more consistent with the general flow).

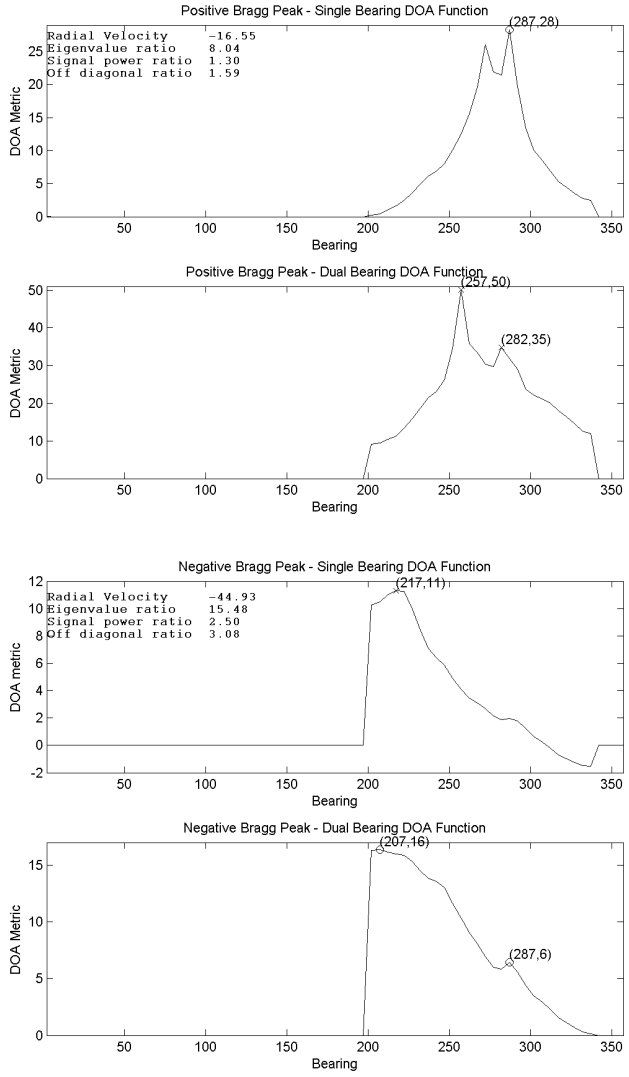

Figure 20 – MUSIC DOA functions for (a,b) a single bearing solution at bearing 287, and (c,d) a dual bearing solution including bearing 287, showing the effect of the irregular measured SDBP antenna pattern on radial velocity output

In Figures 20(c,d), the radial velocity output is -44.93 cm s^{-1}, and the dual bearing solution is chosen (due to eigenvalue and signal power ratios) giving bearings of 207 and 287. Note the smaller local maximum in the dual bearing DOA function, this is due to the irregularity in the antenna manifold at bearing 287. The irregular increase in gain and

shift in phase in the measured antenna pattern has made a second maximum producing an erroneous result. Without the irregularity, the DOA function for the dual bearing result would have been monotonically decreasing from the highest maximum at 207, and only one bearing would have been output. This also reveals the fact that under the dual bearing hypothesis, sometimes only one bearing is produced.

5.1.3 DOA Metric Spatial Distribution

Figure 21 shows the spatial distribution of the DOA metrics for one hour of cross spectra, there is a slight relative decrease in DOA metric magnitude at bearing 287. More noticeable is the dramatic decrease in DOA metric magnitude to the south west at far range.

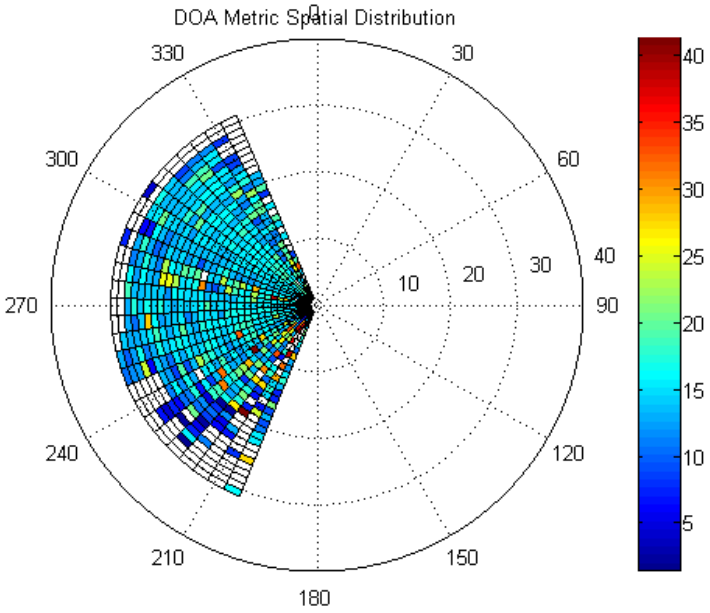

Figure 21 – Spatial distribution of SDBP DOA metrics

6. Edge Effects of the MUSIC Algorithm

6.1 Radial Velocity Vectors Over Land Using Ideal Antenna Patterns

Radial velocity vectors over land come from different sources, the two most common being: 1) use of incorrect phase responses in the antenna manifold, and 2) noise. Land radials from the first source arise when the relative phase responses of the dipole antennas to the monopole antenna used by the MUSIC algorithm are incorrect. An extreme example of this would be to invert (shift by 180 degrees) the phases of the dipoles when doing MUSIC processing. In this case, using the simulation, all the radial velocity vectors that would rightfully be over sea would end up erroneously over land. Operational CODAR users may have encountered this when setting up a system and

initially setting the antenna phase responses. It is assumed that this source of land radials is eliminated by accurate antenna phase response measurements.

The second source of land radials is noise, which can come from various sources (system, interference, targets, secondary scatter, etc.). In the simulation, there is no interference, targets, or secondary scatter, which means that the land radials are all a product of the three simulated sources of AWGN (wind wave, current, and thermal).

In the previous simulated eddy example, MUSIC results over land make up 6.05% of the results, and are erased and never used in the final radial output.

Figure 22 shows some statistical results for single bearing results over land. These can only occur if the antenna manifold is defined over land bearings, as is the case with the 360 degree ideal patterns in use so far. In this run, single results over land (174 results) make up 1.7% of the total results. Figure 22(a) corresponds to the metrics for the single bearing MUSIC results over land. Note that they are distributed lower than the overall metrics in Figure 11(a), with a mean 12.80 dB and a standard deviation of 6.74 dB. Applying a 10 dB minimum DOA metric threshold on all results will eliminate 62 of these results, leaving the contribution of single bearing results over land at 1.1% of the total results, a 0.6% reduction.

Figure 22(b) shows a regular radial velocity distribution, indicating that radials over land can come from processing any Doppler cell, up to the radial velocity limit we impose on the simulation (50 cm/s in this case).

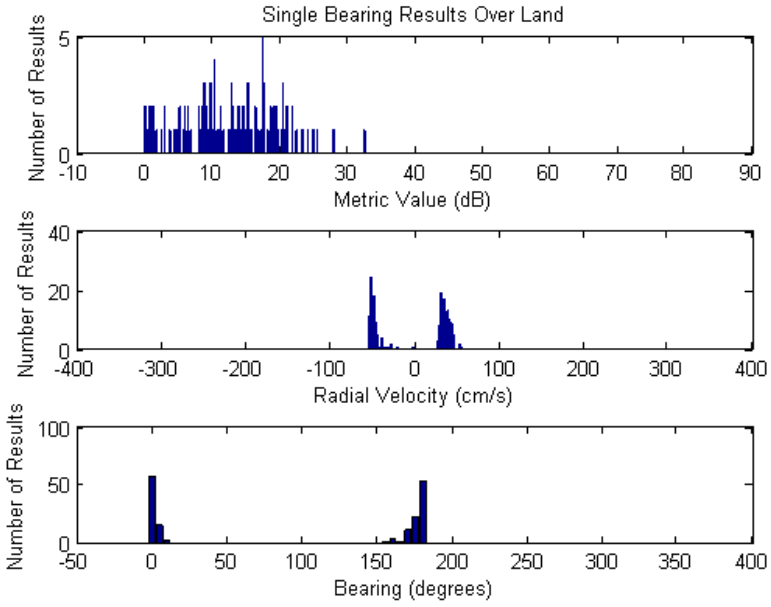

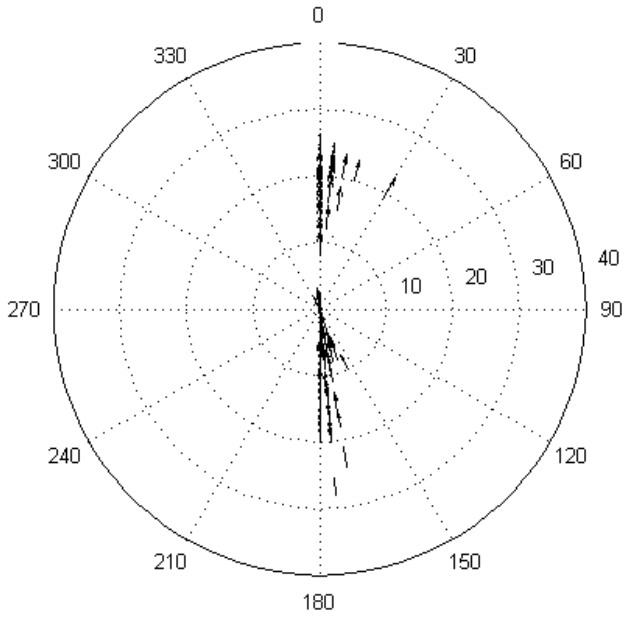

Figure 22 – Single Bearing Results Over Land: (a) DOA Metrics, (b) Radial Velocity Distribution, (c) Bearing Distribution, (d) Spatial Distribution

Figures 22(c,d) show the distributions of the land radials by bearing, where most of them fall on the bearings at the shore, with a scattered few at other bearings. The presence of the results at the shore is further explained in the next section.

Figure 23 corresponds to dual bearing MUSIC results with at least one bearing over land, and only those over land are shown. In this run, the number dual results with both bearings over land (34 results) or at least one bearing over land (411 results) make up 4.35% of the total results. These metrics form similar distribution to the overall DOA metric distribution in 11(a), with a mean of 21.45 dB and a standard deviation of 8.50 dB. Of these results, 419 of the DOA metrics are 10 dB or above, so applying the 10 dB minimum would only eliminate 26 of them, reducing the percentage to 4.10% of the total results, a 0.25% reduction.

Upon closer scrutiny, certainly all the results over land are incorrect. But if we consider the cases where one of the results is over land and one of them is over sea, we can then determine if the results over sea are True Positives or not. If the results over sea are compared to the corresponding (R,θ) inputs, 286 of them (64.3% of the dual results with at least one bearing over land) are True Positives. Therefore if we choose to throw out any dual bearing result with at least one result over land we would eliminate 286 True Positive results and 125 False Positive results. If we go one step further and enforce a minimum DOA metric threshold of 10 dB, 62.8% of the results are True Positives.

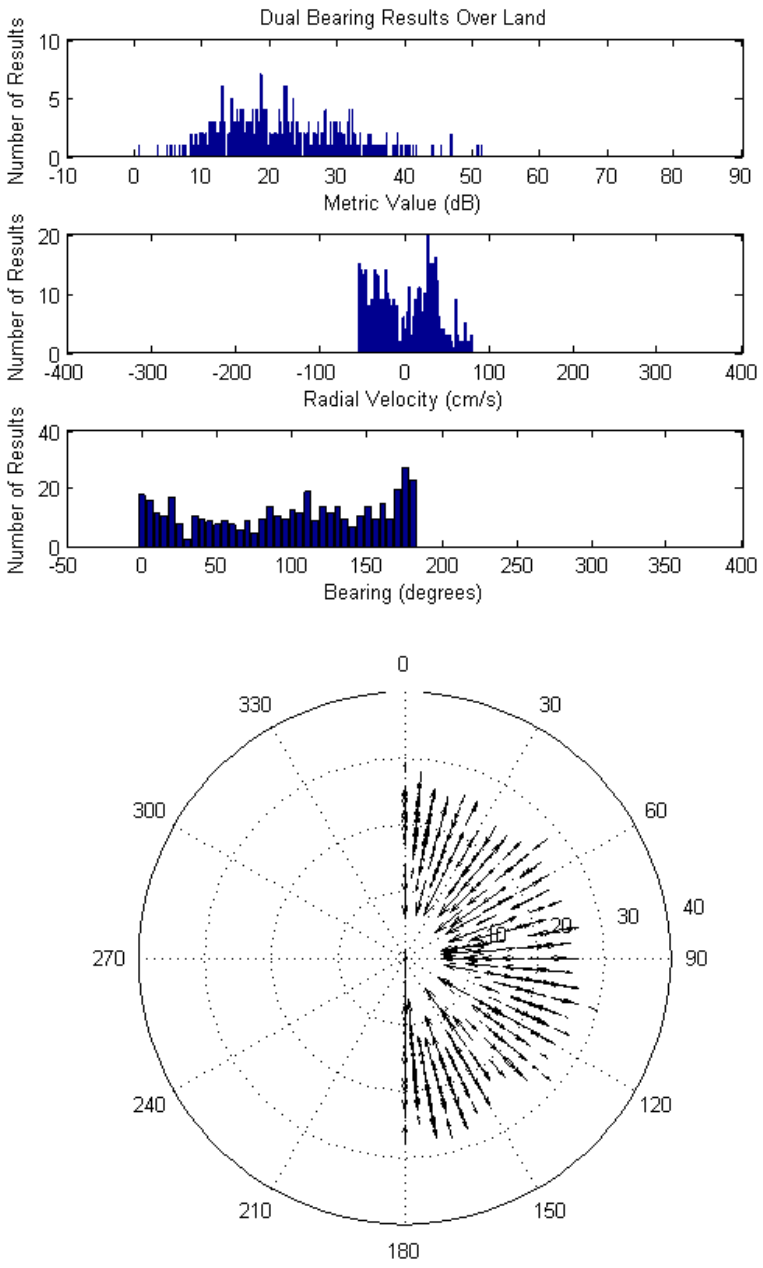

Figure 23 – Dual Bearing Results Over Land: (a) DOA Metrics, (b) Radial Velocity Distribution, (c) Bearing Distribution, (d) Spatial Distribution

So where does that lead us? All of these radial velocity vectors over land bearings are bad output. Using only our goodness-of-fit metric, most of the single bearing results will have low quality and not pass the test, while the double bearing results will have relatively high quality and many will pass the test. Fortunately, all of the results over land are thrown away by masking off all land results. With the added rejection of all double bearing results when at least one is over land, we will only eliminate a small number of "good" results and eliminate many bad ones.

6.2 Clustering of Radials at the Edge of Measured Antenna Patterns

One commonly witnessed phenomenon when using measured antenna patterns is the clustering of radial velocity vectors on the edges of the antenna pattern, at the bearings where the patterns end. For example, typical SDBP output is shown in Figure 24(a). Note the increase in the number of radials (as well as increased range) at the edges of the output, at bearings 202 and 337. The number of radial velocity vectors seems to be tapering off right before those bearings, and yet there are many more vectors right at the edges of coverage. This clustering of radials comes from determining the maxima of the DOA function with truncated antenna patterns. The MUSIC algorithm only produces output for bearings where the antenna patterns are defined. At times when the best MUSIC solution is actually beyond the antenna coverage, the maximum of the DOA function will be at the edge of coverage. This can be seen in Figure 24(c), where a dual angle solution has been determined. The DOA function is increasing toward the lower edge of coverage, and the bearing output is the exact edge of coverage (bearing 202) since that's all the algorithm has to work with. This may be the correct solution, however due to the clustering, it is evident that many of these solutions on the edge of coverage are due to better solutions beyond the edge.

One way to get around the clustering of radials is to extrapolate the measured antenna patterns over land by 5 degrees. We have already seen the existence of radial velocity output over land, and how it is erased before radial data is output. By extending the measured patterns out by 5 degrees on each side, the clustering occurs over the land, and the cluster of radials is erased. Having done this to the SDBP antenna patterns, the radial velocity vectors at the edges of coverage appear more consistent with the field near by, as seen in Figure 24(d).

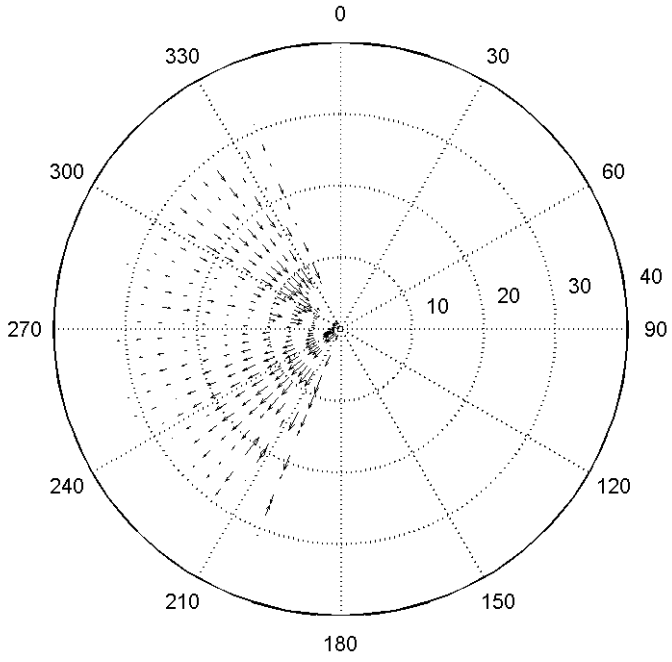

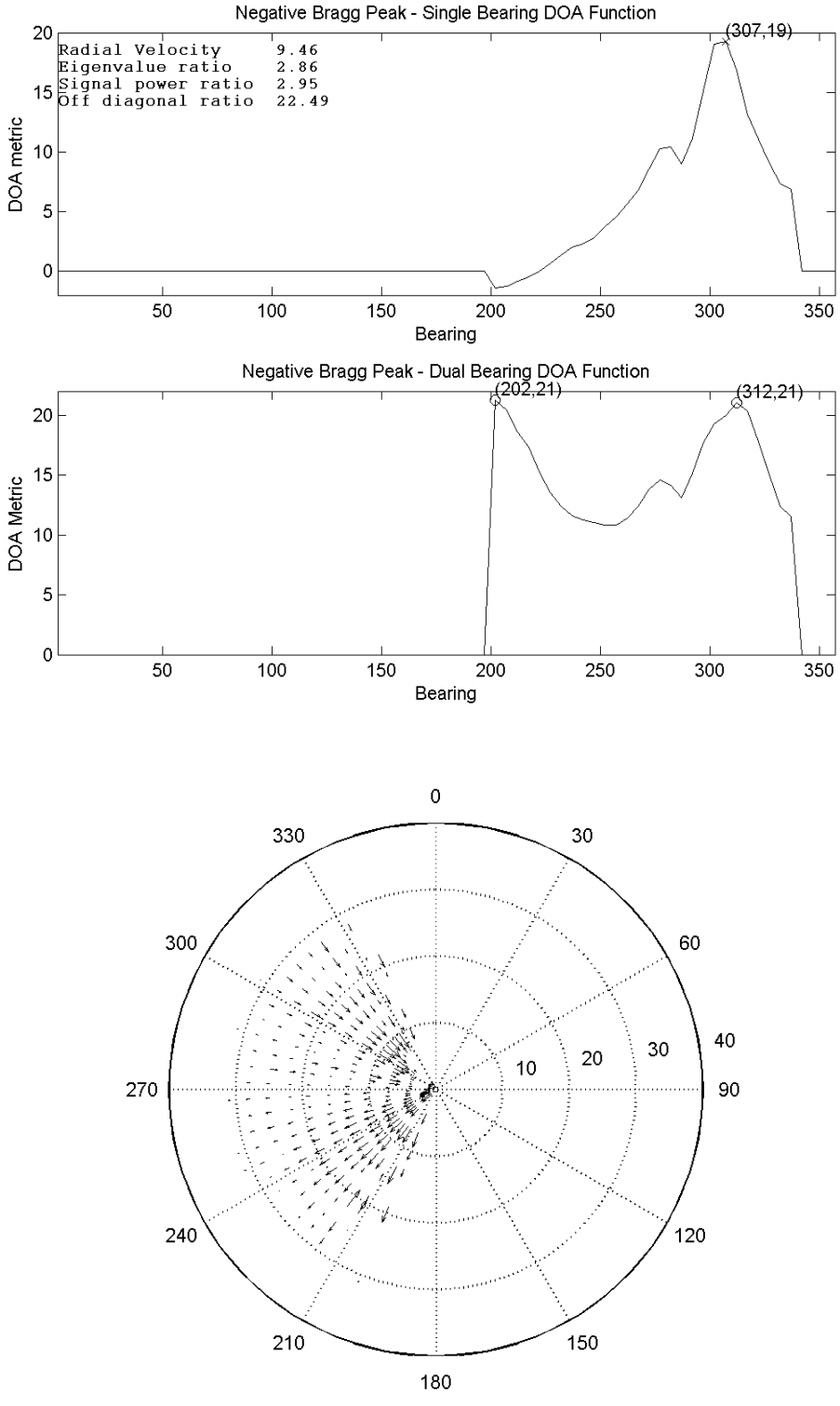

Figure 24 – (a) clustering of radial vectors on the edges of coverage, (b) single bearing DOA function, (c) a dual bearing DOA function producing output at one edge (bearing 202), and (d) radial velocity vector field produced after extrapolating the antenna patterns by 5 degrees over land

7. MUSIC Single/Dual Bearing Parameters

There are currently three parameters used in determining either single or dual bearing results from the MUSIC algorithm. These are commonly known as "MUSIC parameters" and the default values are often listed [20, 10, 3]. The definitions are:

1. Eigenvalue ratio (ER) – the ratio of the largest to the second largest eigenvalues from the covariance matrix diagonalization. Given the diagonal eigenvalue matrix Λ:

$$\Lambda = \begin{bmatrix} \lambda_1 & & \\ & \lambda_2 & \\ & & \lambda_3 \end{bmatrix}$$

$$ER = \frac{\lambda_3}{\lambda_2}$$

   If the ratio ER is less than 20, then a dual bearing solution is possible; the rationale being the larger the second eigenvalue, the higher probability that two signals exist in the covariance matrix.

2. Signal power ratio (PR) – a 2x2 signal power matrix (S) for two hypothetical signals is computed and the diagonal elements are compared according to the following equations. Given that MUSIC has determined two potential bearings for two distinct signals (θ_1 and θ_2), the two corresponding antenna manifold vectors, and the two signal space eigenvectors:

$$G = A^T E_s = \begin{bmatrix} A_1(\theta_1) & A_2(\theta_1) & A_3(\theta_1) \\ A_1(\theta_2) & A_2(\theta_2) & A_3(\theta_2) \end{bmatrix} \begin{bmatrix} E_2(1) & E_3(1) \\ E_2(2) & E_3(2) \\ E_2(3) & E_3(3) \end{bmatrix}$$

$$S = (G^{-1})^T \begin{bmatrix} \lambda_2 & \\ & \lambda_3 \end{bmatrix} G^{-1} = \begin{bmatrix} S_{11} & S_{12} \\ S_{21} & S_{22} \end{bmatrix}$$

$$PR = \frac{S_{22}}{S_{11}}$$

   If PR is less than 10, then a dual bearing solution is possible. Again, the rationale is if there is enough power found in a second signal hypothesis (S_{11}), the higher probability that two signals exist in the covariance matrix.

3. Signal off diagonal power ratio (OD) – using the same equations in (2) above, covariance power is also computed for the two hypothetical signals. If the ratio of the product of the two signal powers (diagonal elements) to the product of the covariance powers (off diagonal elements) is greater than 3, then a dual bearing solution is possible.

$$OD = \frac{S_{11} S_{22}}{S_{12} S_{21}}$$

   The rationale here is that there will be high variance power in the numerator and low covariance power in the denominator if there are two signals, thus the ratio should be larger.

All three of the above three conditions must be satisfied before a dual bearing solution is produced.

7.2 Effects of Varying MUSIC Parameters on Simulated Currents

The effects of varying the defined MUSIC parameters on varying simulated input currents (see de Paolo and Terrill, 2007) are now shown. In general, if the input currents give rise to a higher percentage of dual bearing solutions, then varying the parameters to allow more dual bearing solutions benefits the MUSIC results statistically. With respect to the three defined MUSIC parameters:

1. Increasing/reducing the threshold on ER increases/reduces the number of dual bearing results
2. Increasing/reducing the threshold on PR increases/reduces the number of dual bearing results
3. Increasing/reducing the threshold on OD **reduces/increases** the number of dual bearing results (note this one has the opposite sense).

7.2.1 Onshore Uniform Current

An onshore uniform velocity current aimed directly at the HF RADAR, along with an onshore wind, provides the MUSIC algorithm with many dual bearing velocity inputs. Increasing the thresholds on ER, PR, and decreasing the threshold on OD, gives rise to more dual bearing results and better quality of MUSIC output. In addition, results for a cross-shore wind are shown. In this case the number of dual bearing results are far less, and therefore decreasing the threshold of ER, PR, and increasing the threshold on OD, has a positive effect. To see the effects of changing the MUSIC parameters, look at the TP/FP column to the far right of each table. This is summarized in Appendix A.3.

7.2.2 Along-shore Uniform Current

An along-shore uniform velocity current, under either wind bearing scenario, produces a majority of single bearing MUSIC results. Therefore decreasing the threshold of ER, PR, and increasing the threshold on OD, has a positive effect. To see the effects of changing the MUSIC parameters, look at the TP/FP column to the far right of each table. This is summarized in Appendix A.4.

7.2.3 Along-shore Shear Current

An along-shore shear current, under either wind bearing scenario, produces a majority of single bearing MUSIC results. Therefore decreasing the threshold of ER, PR, and increasing the threshold on OD, has a positive effect. To see the effects of changing the MUSIC parameters, look at the TP/FP column to the far right of each table. This is summarized in Appendix A.5.

7.2.4 Eddy Current

An eddy current, under either wind bearing scenario, produces a majority of single bearing MUSIC results. The eddy produces more dual bearing results than the last two scenarios, but less than the first scenario. Still, decreasing the threshold of ER, PR, and increasing the threshold on OD, has a positive effect. To see the effects of changing the

MUSIC parameters, look at the TP/FP column to the far right of each table. This is summarized in Appendix A.6.

8. References

de Paolo, T., Terrill, E: Skill Assessment of Resolving Ocean Surface Current Structure using Compact-Antenna Style HF RADAR and the MUSIC Direction Finding Algorithm, *American Meteorological Society Journal of Atmospheric and Oceanic Technology*, July 2007.

A. Simulation Results

Sets of simulation results are provided below. Each column is defined by:

- Run – simulation number
- Type – spatial shape of input currents
- U – east-west current velocity (cm/s)
- V – north-south current velocity (cm/s)
- R – radial current velocity (cm/s)
- θ - angular current velocity (cm/s)
- Wind – wind bearing (degrees)
- ER – Eigenvalue ratio defined in Section 7
- PR – Power ratio defined in Section 7
- OD – Off-diagonal power ratio defined in Section 7
- DOAmin – Minimum DOA metric allowed (dB)
- Skill – overall skill, averaged over the spatial field
- RMS – overall RMS error, averaged over the spatial field
- σ - overall standard deviation, averaged over the spatial field
- Single – number of MUSIC single bearing results
- Dual – number of MUSIC dual bearing results
- Land – number of MUSIC results over land
- DOA μ - mean value of all DOA metrics (dB)
- DOA σ - standard deviation of all DOA metrics (dB)
- DG – of all dual bearing results with one result over land, the percentage of the other result in the pair that are true positives
- FP – false positives
- TP – true positives
- TP/FP – ratio of true positives to false positives

A.1 Minimum DOA Metric of 0dB

Results with a DOA metric of 0 dB or higher are accepted (which is basically all of the results).

Run	Type	U	V	R	θ	Wind	Skill	RMS	σ	Single	Dual	Land	DOA μ	DOA σ	DG	FP	TP	TP/FP
1	Uniform	40	0	0	0	270	0.69	6.88	2.32	2120	2031	334	21.96	12.41	0.38	1289	4893	3.80
2	Uniform	40	0	0	0	185	0.75	5.76	1.91	4045	525	228	20.74	7.82	0.55	437	4658	10.66
3	Uniform	0	40	0	0	270	0.73	6.38	2.23	7015	374	322	24.35	8.53	0.62	592	7171	12.11
4	Uniform	0	-40	0	0	185	0.73	6.23	2.16	6880	377	314	24.73	8.75	0.72	553	7081	12.80
5	Uniform	40	40	0	0	270	0.73	9.07	2.69	7364	752	511	24.81	10.15	0.49	1013	7855	7.75
6	Uniform	40	-40	0	0	185	0.74	8.31	2.42	6382	678	462	25.11	10.54	0.56	861	6877	7.99
7	Uniform	-40	40	0	0	270	0.71	9.41	2.69	7355	717	426	24.85	10.12	0.57	912	7877	8.64
8	Uniform	-40	-40	0	0	185	0.74	8.70	2.41	6587	674	399	25.18	10.49	0.55	775	7160	9.24
9	Shear	40	0	0	0	270	0.72	4.61	1.79	1210	1179	268	19.11	11.35	0.50	583	2985	5.12
10	Shear	-40	0	0	0	185	0.72	4.60	1.54	2080	420	156	19.69	8.13	0.40	288	2632	9.14
11	Shear	0	40	0	0	270	0.70	5.20	1.77	3642	389	265	21.53	8.27	0.71	446	3974	8.91
12	Shear	0	-40	0	0	185	0.71	4.88	1.72	3584	377	222	21.87	8.46	0.71	423	3915	9.26
13	Shear	40	40	0	0	270	0.67	6.25	2.08	4358	670	422	22.23	8.65	0.55	834	4864	5.83
14	Shear	40	-40	0	0	185	0.68	5.86	2.00	4038	592	380	22.26	8.88	0.56	714	4508	6.31
15	Shear	-40	40	0	0	270	0.68	5.71	2.01	4208	583	354	22.13	8.54	0.55	746	4628	6.20
16	Shear	-40	-40	0	0	185	0.68	5.93	2.04	3905	628	329	22.26	8.80	0.53	739	4422	5.98
17	Eddy	40	0	20	200	270	0.57	6.54	3.09	4742	2478	539	21.79	12.26	0.55	1917	7781	4.06
18	Eddy	-40	0	20	200	185	0.71	9.97	2.38	4391	786	412	19.42	8.31	0.60	985	4978	5.05
19	Eddy	0	40	20	200	270	0.63	8.92	2.75	6662	877	370	23.82	9.82	0.62	1126	7290	6.47
20	Eddy	0	-40	20	200	185	0.73	8.07	2.53	6051	498	305	24.95	9.81	0.68	617	6430	10.42
21	Eddy	40	40	20	200	270	0.68	9.61	3.14	7819	1214	615	23.61	10.95	0.51	1452	8795	6.06
22	Eddy	40	-40	20	200	185	0.69	8.86	3.11	8388	888	515	24.61	10.72	0.53	1184	8980	7.58
23	Eddy	-40	40	20	200	270	0.69	10.87	2.77	6964	975	450	23.71	9.57	0.54	1249	7665	6.14
24	Eddy	-40	-40	20	200	185	0.69	10.68	2.80	6374	612	424	24.17	9.79	0.58	875	6723	7.68
25	Eddy	40	0	20	-200	270	0.57	6.76	3.09	4610	2543	527	22.22	12.41	0.55	1869	7827	4.19
26	Eddy	0	40	20	-200	185	0.72	8.37	2.54	6144	485	314	24.97	9.84	0.70	602	6512	10.82
27	Eddy	40	40	20	-200	270	0.69	9.49	3.19	9540	1175	674	24.31	10.62	0.50	1507	10383	6.89
28	Eddy	-40	-40	20	-200	185	0.67	11.97	2.87	6490	795	360	23.78	9.82	0.60	1088	6992	6.43
29	Eddy	40	0	-20	200	270	0.72	9.10	2.48	3499	1276	434	18.74	9.47	0.62	1113	4938	4.44
30	Eddy	0	40	-20	200	185	0.63	8.83	2.76	6146	720	305	24.00	10.01	0.63	1003	6583	6.56
31	Eddy	40	40	-20	200	270	0.66	12.16	2.85	7091	911	426	23.21	9.58	0.55	1318	7595	5.76
32	Eddy	-40	-40	-20	200	185	0.70	8.77	3.14	8360	937	502	24.76	10.83	0.52	1195	9039	7.56

A.2 Minimum DOA Metric of 10dB

Results with DOA metrics of 10 dB or higher are accepted, eliminating results with low metrics.

Run	Type	U	V	R	θ	Wind	Skill	RMS	σ	Single	Dual	Land	DOA μ	DOA σ	DG	FP	TP	TP/FP
1	Uniform	40	0	0	0	270	0.71	6.71	1.91	1033	1865	218	26.7	9.44	0.42	519	4244	8.18
2	Uniform	40	0	0	0	185	0.73	6.56	1.85	3882	394	198	21.83	6.94	0.26	320	4350	13.59
3	Uniform	0	40	0	0	270	0.72	6.45	2.03	6926	204	320	25.32	7.64	0.36	477	6857	14.38
4	Uniform	0	-40	0	0	185	0.71	6.51	2.02	6791	182	275	25.95	7.76	0.35	418	6737	16.12
5	Uniform	40	40	0	0	270	0.69	10.26	2.55	7135	523	445	26.13	9.11	0.31	760	7421	9.76
6	Uniform	40	-40	0	0	185	0.72	9.26	2.28	6223	512	378	26.85	9.71	0.31	622	6625	10.65
7	Uniform	-40	40	0	0	270	0.71	9.35	2.35	7081	551	418	26.21	9.11	0.35	716	7467	10.43
8	Uniform	-40	-40	0	0	185	0.71	9.28	2.34	6320	522	363	26.66	9.31	0.38	597	6767	11.34
9	Shear	40	0	0	0	270	0.71	4.89	1.5	477	995	170	24.2	8.15	0.51	281	2186	7.78
10	Shear	-40	0	0	0	185	0.73	4.58	1.47	1852	385	162	21.07	7.19	0.26	251	2371	9.45
11	Shear	0	40	0	0	270	0.68	5.53	1.69	3512	238	232	22.84	7.08	0.41	342	3646	10.66
12	Shear	0	-40	0	0	185	0.69	5.87	1.6	3488	272	223	23.19	7.31	0.41	385	3647	9.47
13	Shear	40	40	0	0	270	0.67	6.41	2.01	4210	506	399	23.63	7.44	0.37	689	4533	6.58
14	Shear	40	-40	0	0	185	0.67	6.47	1.84	3871	432	292	23.73	7.43	0.34	560	4175	7.46
15	Shear	-40	40	0	0	270	0.64	6.93	1.98	4008	490	331	23.53	7.49	0.39	633	4355	6.88
16	Shear	-40	-40	0	0	185	0.67	6.38	1.86	3714	470	289	23.79	7.65	0.35	544	4110	7.56
17	Eddy	40	0	20	200	270	0.58	5.94	2.72	3265	2284	396	26.13	10.08	0.41	1052	6781	6.45
18	Eddy	-40	0	20	200	185	0.7	10.71	2.29	4004	515	335	21.38	6.89	0.34	632	4402	6.97
19	Eddy	0	40	20	200	270	0.6	9.63	2.74	6418	636	360	25.41	8.7	0.29	878	6812	7.76
20	Eddy	0	-40	20	200	185	0.71	8.23	2.41	5849	371	319	26.31	8.94	0.42	511	6080	11.90
21	Eddy	40	40	20	200	270	0.66	10.51	2.98	7266	949	534	25.73	9.73	0.28	1102	8062	7.32
22	Eddy	40	-40	20	200	185	0.67	9.54	3.04	7990	651	465	26.14	9.93	0.26	892	8400	9.42
23	Eddy	-40	40	20	200	270	0.65	12.65	2.8	6635	720	346	25.14	8.4	0.32	948	7127	7.52
24	Eddy	-40	-40	20	200	185	0.67	11.51	2.5	6133	407	375	25.87	8.74	0.37	661	6286	9.51
25	Eddy	40	0	20	-200	270	0.58	6.07	2.75	3288	2262	420	26.15	10.09	0.39	1098	6714	6.11
26	Eddy	0	40	20	-200	185	0.7	8.78	2.47	6104	336	265	26.22	8.72	0.41	473	6303	13.33
27	Eddy	40	40	20	-200	270	0.68	9.41	2.99	9218	881	570	25.88	9.72	0.29	1089	9891	9.08
28	Eddy	-40	-40	20	-200	185	0.67	11.81	2.62	6201	571	348	25.24	8.67	0.29	850	6493	7.64
29	Eddy	40	0	-20	200	270	0.71	9.68	2.36	2823	1060	376	22.3	7.66	0.45	800	4143	5.18
30	Eddy	0	40	-20	200	185	0.62	8.99	2.61	5971	508	302	25.35	8.88	0.35	767	6220	8.11
31	Eddy	40	40	-20	200	270	0.67	11.93	2.71	6694	690	389	24.93	8.32	0.28	915	7159	7.82
32	Eddy	-40	-40	-20	200	185	0.69	9.32	2.86	8077	656	436	26.23	9.87	0.28	851	8538	10.03

A.3 Effects of Varying MUSIC Parameters on an Onshore Uniform Current

Results are shown for varying values of ER, PR, and OD. With an onshore wind (bearing 270), there are many dual bearing results. Increasing the thresholds on ER and PR, and decreasing the threshold on OD, produces more dual bearing results. An increase in performance is seen in the TP/FP column on the far right. In general, TP/FP goes up when more dual bearing results are produced. With a cross-shore wind (bearing 185), there are more single and less dual bearing results. Allowing for more single bearing results has a better effect in this case.

Run	Type	U	V	R	θ	Wind	ER	PR	OD	Skill	RMS	σ	Single	Dual	Land	DOAμ	DOAσ	DG	FP	TP	TP/FP
1	Uniform	40	0	0	0	270	40	10	3.0	0.69	6.95	2.39	2067	2083	396	22.15	12.70	0.39	1284	4949	3.85
2	Uniform	40	0	0	0	270	20	10	3.0	0.68	7.27	2.40	2142	1968	344	21.92	12.53	0.38	1245	4833	3.88
3	Uniform	40	0	0	0	270	10	10	3.0	0.67	7.59	2.43	2337	1778	323	21.01	12.52	0.40	1288	4605	3.58
4	Uniform	40	0	0	0	270	20	20	3.0	0.68	7.28	2.48	2093	2044	340	21.83	12.57	0.41	1251	4930	3.94
2	Uniform	40	0	0	0	270	20	10	3.0	0.68	7.27	2.40	2142	1968	344	21.92	12.53	0.38	1245	4833	3.88
5	Uniform	40	0	0	0	270	20	5	3.0	0.68	7.17	2.42	2333	1815	275	21.28	12.43	0.32	1203	4760	3.96
6	Uniform	40	0	0	0	270	20	10	6.0	0.66	7.67	2.50	2905	1194	303	18.26	12.92	0.24	1344	3949	2.94
2	Uniform	40	0	0	0	270	20	10	3.0	0.68	7.27	2.40	2142	1968	344	21.92	12.53	0.38	1245	4833	3.88
7	Uniform	40	0	0	0	270	20	10	1.5	0.72	6.38	2.19	1228	2915	388	25.33	10.95	0.55	1030	6028	5.85
8	Uniform	40	0	0	0	185	40	10	3.0	0.75	5.82	2.00	4012	597	227	21.12	8.23	0.50	444	4762	10.73
9	Uniform	40	0	0	0	185	20	10	3.0	0.74	6.16	1.86	4018	509	219	20.92	7.84	0.43	448	4588	10.24
10	Uniform	40	0	0	0	185	10	10	3.0	0.76	5.71	1.84	4325	303	241	20.02	7.21	0.43	411	4520	11.00
11	Uniform	40	0	0	0	185	20	20	3.0	0.75	5.78	1.88	3920	657	281	21.02	8.05	0.59	505	4729	9.36
9	Uniform	40	0	0	0	185	20	10	3.0	0.74	6.16	1.86	4018	509	219	20.92	7.84	0.43	448	4588	10.24
12	Uniform	40	0	0	0	185	20	5	3.0	0.75	5.79	1.90	4300	269	157	20.24	7.22	0.28	341	4497	13.19
13	Uniform	40	0	0	0	185	20	10	6.0	0.75	5.61	1.85	4289	275	183	20.22	7.36	0.35	346	4493	12.99
9	Uniform	40	0	0	0	185	20	10	3.0	0.74	6.16	1.86	4018	509	219	20.92	7.84	0.43	448	4588	10.24
14	Uniform	40	0	0	0	185	20	10	1.5	0.76	5.73	1.98	3895	717	291	21.27	8.05	0.53	523	4806	9.19

A.4 Effects of Varying MUSIC Parameters on a Along-shore Uniform Current

Results are shown for varying values of ER, PR, and OD. Under both wind bearing scenarios, allowing for more single bearing results has a positive effect in the TP/FP column.

Run	Type	U	V	R	θ	Wind	ER	PR	OD	Skill	RMS	σ	Single	Dual	Land	DOAμ	DOAσ	DG	FP	TP	TP/FP
15	Uniform	0	40	0	0	270	40	10	3.0	0.72	6.70	2.19	6985	365	302	24.42	8.60	0.70	535	7180	13.42
16	Uniform	0	40	0	0	270	20	10	3.0	0.73	6.36	2.11	7035	386	337	24.21	8.63	0.75	540	7267	13.46
17	Uniform	0	40	0	0	270	10	10	3.0	0.74	5.94	2.01	7141	231	236	24.41	8.59	0.59	424	7179	16.93
18	Uniform	0	40	0	0	270	20	20	3.0	0.72	6.76	2.29	6808	495	425	24.14	8.69	0.74	685	7113	10.38
16	Uniform	0	40	0	0	270	20	10	3.0	0.73	6.36	2.11	7035	386	337	24.21	8.63	0.75	540	7267	13.46
19	Uniform	0	40	0	0	270	20	5	3.0	0.74	6.11	1.98	7234	168	150	24.45	8.40	0.51	354	7216	20.38
20	Uniform	0	40	0	0	270	20	10	6.0	0.75	5.65	1.93	7204	198	203	24.36	8.55	0.68	358	7242	20.23
16	Uniform	0	40	0	0	270	20	10	3.0	0.73	6.36	2.11	7035	386	337	24.21	8.63	0.75	540	7267	13.46
21	Uniform	0	40	0	0	270	20	10	1.5	0.73	6.77	2.27	6827	469	386	24.36	8.43	0.70	657	7108	10.82
22	Uniform	0	40	0	0	185	40	10	3.0	0.72	6.35	2.12	6770	367	296	24.72	8.56	0.74	523	6981	13.35
23	Uniform	0	40	0	0	185	20	10	3.0	0.74	5.69	2.02	6639	322	277	24.60	8.48	0.71	478	6805	14.24
24	Uniform	0	40	0	0	185	10	10	3.0	0.74	5.85	1.85	6777	199	191	24.79	8.40	0.72	320	6855	21.42
25	Uniform	0	40	0	0	185	20	20	3.0	0.72	6.75	2.14	6624	421	338	24.72	8.49	0.78	572	6894	12.05
23	Uniform	0	40	0	0	185	20	10	3.0	0.74	5.69	2.02	6639	322	277	24.60	8.48	0.71	478	6805	14.24
26	Uniform	0	40	0	0	185	20	5	3.0	0.73	5.88	1.91	6905	164	122	24.99	8.26	0.66	316	6917	21.89
27	Uniform	0	40	0	0	185	20	10	6.0	0.72	6.03	1.92	6779	191	170	24.64	8.50	0.71	333	6828	20.50
23	Uniform	0	40	0	0	185	20	10	3.0	0.74	5.69	2.02	6639	322	277	24.60	8.48	0.71	478	6805	14.24
28	Uniform	0	40	0	0	185	20	10	1.5	0.72	6.95	2.23	6547	508	401	24.61	8.52	0.74	691	6872	9.95

A.5 Effects of Varying MUSIC Parameters on a Along-shore Shear Current

Results are shown for varying values of ER, PR, and OD. Under both wind bearing scenarios, allowing for more single bearing results has a positive effect in the TP/FP column.

Run	Type	U	V	R	θ	Wind	ER	PR	OD	Skill	RMS	σ	Single	Dual	Land	DOAμ	DOAσ	DG	FP	TP	TP/FP
29	Shear	0	40	0	0	270	40	10	3.0	0.72	4.86	1.78	3528	489	293	22.24	8.67	0.72	479	4027	8.41
30	Shear	0	40	0	0	270	20	10	3.0	0.70	5.08	1.81	3648	361	234	21.66	8.26	0.65	440	3930	8.93
31	Shear	0	40	0	0	270	10	10	3.0	0.72	4.70	1.67	3793	218	194	21.05	7.73	0.61	341	3888	11.40
32	Shear	0	40	0	0	270	20	20	3.0	0.70	4.91	1.82	3575	450	349	21.28	8.25	0.71	522	3953	7.57
30	Shear	0	40	0	0	270	20	10	3.0	0.70	5.08	1.81	3648	361	234	21.66	8.26	0.65	440	3930	8.93
33	Shear	0	40	0	0	270	20	5	3.0	0.71	5.04	1.73	3751	242	183	21.44	8.07	0.51	338	3897	11.53
34	Shear	0	40	0	0	270	20	10	6.0	0.72	4.77	1.71	3811	225	173	21.28	8.08	0.57	332	3929	11.83
30	Shear	0	40	0	0	270	20	10	3.0	0.70	5.08	1.81	3648	361	234	21.66	8.26	0.65	440	3930	8.93
35	Shear	0	40	0	0	270	20	10	1.5	0.69	5.34	1.87	3545	490	329	21.87	8.22	0.64	563	3962	7.04
36	Shear	0	40	0	0	185	40	10	3.0	0.71	5.19	1.73	3476	476	225	22.56	8.88	0.76	456	3972	8.71
37	Shear	0	40	0	0	185	20	10	3.0	0.71	5.02	1.73	3552	411	254	22.03	8.30	0.73	481	3893	8.09
38	Shear	0	40	0	0	185	10	10	3.0	0.70	5.14	1.68	3803	239	194	21.38	7.94	0.69	371	3910	10.54
39	Shear	0	40	0	0	185	20	20	3.0	0.69	5.31	1.78	3546	435	276	21.84	8.32	0.82	458	3958	8.64
37	Shear	0	40	0	0	185	20	10	3.0	0.71	5.02	1.73	3552	411	254	22.03	8.30	0.73	481	3893	8.09
40	Shear	0	40	0	0	185	20	5	3.0	0.71	4.84	1.70	3715	289	156	21.84	8.19	0.67	360	3933	10.93
41	Shear	0	40	0	0	185	20	10	6.0	0.71	5.11	1.58	3700	249	164	21.68	8.21	0.71	340	3858	11.35
37	Shear	0	40	0	0	185	20	10	3.0	0.71	5.02	1.73	3552	411	254	22.03	8.30	0.73	481	3893	8.09
42	Shear	0	40	0	0	185	20	10	1.5	0.68	6.00	1.77	3491	524	309	22.34	8.40	0.76	554	3985	7.19

A.6 Effects of Varying MUSIC Parameters on an Eddy Current

Results are shown for varying values of ER, PR, and OD. Under both wind bearing scenarios, allowing for more single bearing results has a positive effect in the TP/FP column, although not as dramatic as in the previous two sections, since the dual bearing results are more prevalent in an eddy.

Run	Type	U	V	R	θ	Wind	ER	PR	OD	Skill	RMS	σ	Single	Dual	Land	DOAμ	DOAσ	DG	FP	TP	TP/FP
43	Eddy	40	40	20	200	270	40	10	3.0	0.68	9.21	3.22	7644	1389	637	23.99	11.13	0.48	1583	8839	5.58
44	Eddy	40	40	20	200	270	20	10	3.0	0.66	9.86	3.30	7790	1268	624	23.96	10.97	0.46	1563	8763	5.61
45	Eddy	40	40	20	200	270	10	10	3.0	0.67	9.82	3.04	8112	785	465	23.24	10.65	0.43	1263	8419	6.67
46	Eddy	40	40	20	200	270	20	20	3.0	0.67	10.02	3.21	7585	1409	697	23.95	11.00	0.51	1599	8804	5.51
44	Eddy	40	40	20	200	270	20	10	3.0	0.66	9.86	3.30	7790	1268	624	23.96	10.97	0.46	1563	8763	5.61
47	Eddy	40	40	20	200	270	20	5	3.0	0.70	8.84	2.97	8220	815	431	23.63	10.78	0.31	1194	8656	7.25
48	Eddy	40	40	20	200	270	20	10	6.0	0.68	9.21	2.98	8333	716	449	23.19	10.88	0.40	1262	8503	6.74
44	Eddy	40	40	20	200	270	20	10	3.0	0.66	9.86	3.30	7790	1268	624	23.96	10.97	0.46	1563	8763	5.61
49	Eddy	40	40	20	200	270	20	10	1.5	0.66	10.46	3.24	7462	1585	681	24.49	10.83	0.46	1622	9010	5.55
50	Eddy	40	40	20	200	185	40	10	3.0	0.68	8.99	3.00	6782	1156	500	24.34	11.31	0.57	1259	7835	6.22
51	Eddy	40	40	20	200	185	20	10	3.0	0.68	8.93	2.96	6990	971	497	23.82	11.15	0.56	1264	7668	6.07
52	Eddy	40	40	20	200	185	10	10	3.0	0.68	8.70	2.97	7347	630	398	23.49	10.93	0.47	1103	7504	6.80
53	Eddy	40	40	20	200	185	20	20	3.0	0.66	9.52	3.10	6786	1135	607	23.96	11.18	0.58	1421	7635	5.37
51	Eddy	40	40	20	200	185	20	10	3.0	0.68	8.93	2.96	6990	971	497	23.82	11.15	0.56	1264	7668	6.07
54	Eddy	40	40	20	200	185	20	5	3.0	0.69	8.59	2.82	7423	601	356	23.76	11.07	0.41	982	7643	7.78
55	Eddy	40	40	20	200	185	20	10	6.0	0.69	8.70	2.92	7362	607	391	23.50	11.18	0.47	1032	7544	7.31
51	Eddy	40	40	20	200	185	20	10	3.0	0.68	8.93	2.96	6990	971	497	23.82	11.15	0.56	1264	7668	6.07
56	Eddy	40	40	20	200	185	20	10	1.5	0.66	9.83	3.11	6646	1303	592	24.57	11.00	0.60	1380	7872	5.70